Polymer Testing 138 (2024) 108536

Contents lists available at ScienceDirect

Polymer Testing

journal homepage: www.elsevier.com/locate/polytest

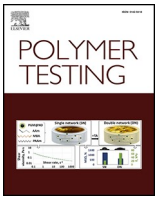

A comprehensive study on the degradation process of medical-grade polydioxanone at low pH

Krisztina Dodzi Lelkes [a], Daniel Jezbera [a,b], Roman Svoboda [c], Štěpán Podzimek [d], Jan Loskot [b], Martina Nalezinková [e], Petr Voda [a], Piotr Duda [f], Alena Myslivcová Fučíková [e], Tomáš Hosszú [g], Dino Alferi [a], Aleš Bezrouk [a,*]

[a] Department of Medical Biophysics, Faculty of Medicine in Hradec Králové, Charles University, 500 03, Hradec Králové, Czech Republic
[b] Department of Physics, Faculty of Science, University of Hradec Králové, Rokitanského 62, 500 03, Hradec Králové, Czech Republic
[c] Department of Physical Chemistry, Faculty of Chemical Technology, University of Pardubice, Studentská 573, 532 10, Pardubice, Czech Republic
[d] Institute of Chemistry and Technology of Macromolecular Materials, Faculty of Chemical Technology, University of Pardubice, Studentská 573, 532 10, Pardubice, Czech Republic
[e] Department of Biology, Faculty of Science, University of Hradec Králové, Rokitanského 62, 500 03, Hradec Králové, Czech Republic
[f] Institute of Biomedical Engineering, University of Silesia in Katowice, Będzińska 39, 41-205, Sosnowiec, Poland
[g] Department of Neurosurgery, University Hospital Hradec Králové, Sokolská 581, 500 05, Hradec Králové, Czech Republic

ARTICLE INFO

Keywords:
Polydioxanone degradation
Size exclusion chromatography
Differential scanning calorimetry
Raman spectroscopy
Elastic modulus
Tensile strength

ABSTRACT

Polydioxanone (PPDX) has gained significant attention as a biocompatible and absorbable polymer used in various medical applications, such as sutures and tissue scaffolds. This research presents a thorough investigation into the degradation mechanisms of PPDX under low pH conditions, simulating physiological environments, *e.g.*, esophagus and stomach. It mainly focuses on the dependence of the PPDX degradation rate on various ambient pH values (7.4 and below), which is a substantial knowledge for successful gastrointestinal treatment. The PPDX suture samples were degraded for up to 6 weeks and analyzed using size exclusion chromatography, differential scanning calorimetry, Raman spectroscopy, scanning electron microscopy, X-ray microtomography, and mechanical property measurements. The results show that the PPDX degradation is significantly accelerated at pH below 1.67. Correlations of the molecular weight, crystallinity, glass transition temperature, Young's modulus, shear modulus, tensile strength, and the 1733 cm^{-1} Raman peak shoulder area (RPSA1733) indicate that the degradation mechanism does not change with increasing acidity. Measurements of tensile strength, shear modulus, and RPSA1733 were found to be the most suitable parameters for characterizing the PPDX filament's macroscopic integrity. Raman spectroscopy is of particular interest in this regard due to its rapidity and practically no requirements on the sample preparation.

1. Introduction

Polydioxanone (PPDX) is a bioabsorbable polymer developed especially for sutures used in wound closure [1]. PPDX is widely accepted for use in the field of medical implants because of its unique qualities and medical safety. In the current practice, biodegradable stent implants are manufactured from this material, too. Many hollow organs with lumen, including bile ducts [2–5], intestine [6], trachea [7–9], and esophagus [10–12], can be treated with polydioxanone stents. Another application of PPDX in medicine is fixation in the form of pins and tiny plates [13]. This polymer is also used experimentally as tissue scaffolds [14] or drug delivery systems [15].

PPDX, as a semi-crystalline and thermoplastic polymer, has highly desirable properties, including histoconductivity, resorbability, and biocompatibility [16]. The poly(ether-ester) molecular structure of PPDX ($(–O–CH_2–CH_2–O–CH2–C=O)_n$) is derived from the monomer paradioxanone by ring-opening polymerization using heat and an organometallic catalyst [17]. This polymer has a pretty good shape memory, and its orthorhombic lattice ($P2_12_12_1$)-shaped crystalline part can take up to 60 % of the polymer structure [18–20]. The glass transition temperature of PPDX ranges from −10 to 0 °C, and its melting temperature is between 110 and 115 °C [1,21,22].

* Corresponding author.
E-mail address: bezrouka@lfhk.cuni.cz (A. Bezrouk).

https://doi.org/10.1016/j.polymertesting.2024.108536
Received 19 June 2024; Received in revised form 23 July 2024; Accepted 3 August 2024
Available online 6 August 2024

The degradation of PPDX is hydrolytic. It is determined by the level of crystallinity, because hydrolysis preferentially occurs in the amorphous parts of the polymer [21,23]. The crystalline parts degrade only after the amorphous parts have already been hydrolyzed [21]. This phenomenon results in a change in the ratio between the amorphous and crystalline phases, thus also affecting mechanical properties [19]. The changes in the mechanical properties of esophageal [24] and intravascular [25] PPDX stents have been studied, including shear and Young's modulus, radial force, fiber elongation, and stent force relaxation. These studies found that the initial degradation of the amorphous phase causes an increase in the radial force [24]. According to Rejchrt et al., a PPDX stent implanted in the gastrointestinal system kept its qualities, including its radial force and integrity, for 6–8 weeks before disintegrating for good after 11–12 weeks [26]. An investigation conducted by Lin et al. found that when exposed to phosphate-buffered saline (PBS), PPDX sutures lost around 67 % of their tensile strength within 14–28 days, with just a little reduction in tensile strength in 42–62 days. Changes in the surface and thermal properties and dye leaching were detected during this investigation, too [21]. The dye leaching was also observed by Loskot et al. [27,28] when studying PPDX stent degradation using Raman spectroscopy.

As mentioned above, polydioxanone implants are widely used in the medical field. One of the application areas is the esophagus, which is often affected by gastroesophageal reflux (GER). Gastroesophageal reflux is the retrograde flow of gastric contents into the esophagus [29]. The pH of human gastric acid is relatively low (below 2.0) [30], so the GER can decrease pH in the esophagus, thus possibly affecting the degradation rate and clinical effect of the PPDX stent.

To the best of our knowledge, only one study has been performed on the degradation of PPDX sutures. This study included only one pH value at the acidic level (pH 1), and the degradation process was studied using a limited number of methods [31]. Therefore, there is a need to study such degradations more thoroughly, so we can better understand how the PPDX degrades at lower, acidic pH levels. This study aims to provide a comprehensive insight into the degradation process of a medical-grade polydioxanone and the underlying thermomechanical and molecular processes, especially with respect to low pH.

2. Materials

Surgical sutures made of polydioxanone were used as research samples (Surgicryl Monofilament; SMI, Sankt Vith, Belgium). Degradation of the sutures was carried out in solutions of different pH. Solutions of pH 1.0 (pH buffer; CARL ROTH, Karlsruhe, Germany); 1.20 (Simulated Gastric Fluids; J.T. Baker, Phillipsburg, New Jersey); 1.67 (pH buffer; CARL ROTH, Karlsruhe, Germany); 3.78 (pH buffer; CARL ROTH, Karlsruhe, Germany); 7.0 (pH buffer; CARL ROTH, Karlsruhe, Germany), and 7.4 (PBS; CARL ROTH, Karlsruhe, Germany) were tested.

3. Experimental

3.1. Degradation

For each pH, a total of 30 pieces of suture (22 pieces of 10 cm length and 8 pieces of 5 cm length) were prepared for one degradation period. Thus obtained samples were placed in 50 ml test tubes filled with the appropriate solutions. The periods of degradation were as follows: 0 weeks (non-degraded samples), 3 days, 1 week, 2 weeks, 3 weeks, 4 weeks, 5 weeks, and 6 weeks. In the following text, we refer to the individual samples as "pH x – y W", where x denotes the pH value of the solution used, and y is the degradation period in weeks. For example, a sample labeled "pH 1.0–2 W" was degraded for 2 weeks in the pH 1.0 solution.

The tubes were shaken all the time in a circular vibrating shaker Vibramax 100 (Heidolph, Schwabach, Germany) placed in a thermostatic cabinet Liebherr FK 3640 (Liebherr Haushaltsgeräte, Ochsenhausen, Germany) at a constant temperature of 37 °C. All sutures were removed and air-dried for 1 h under aseptic conditions in a safety cabinet Safemate EVO 1.2 (BioAir, Camden, NJ, USA) after their degradation period. The samples were then stored in tubes with silica gel and subjected to further analyses as soon as possible.

The pH of all solutions, including control buffers, was continuously measured during the research. These control buffers were exposed to the same incubation conditions (but without contact with the samples) for the entire duration of the study. The pH measurement was performed using a pH meter EDGE (Hanna Instruments Czech s.r.o., Prague, Czech Republic).

The measured pH values were almost constant during the degradation process. They differed from their nominal values by less than 0.1. The pH values for all degradation solutions are provided in Supplementary Materials.

3.2. Molar mass distribution

Molar mass distribution was determined by size exclusion chromatography (SEC; gel permeation chromatography) with a multi-angle light scattering detector (MALS).

The instrumentation used consisted of the following instruments: Agilent 1200 Series Isocratic Pump and Agilent 1200 Series Autosampler; a MALS detector HELEOS and a differential refractometer (RI detector) Optilab T-rEX, both from Wyatt Technology; data acquisition and evaluation were performed using the ASTRA software from Wyatt Technology. Two Shodex HFIP-806 M 300 × 8 mm columns with hexafluoroisopropanol (HFIP) at a flow rate of 1 ml/min as mobile phase were used for the separation. Samples were prepared as solutions in HFIP at a concentration of ≈4 mg/ml and injected in volumes of 100 μl. The used HFIP was modified by the addition of 0.02 M CF_3COONa.

3.3. Thermal analysis

Calorimetric measurements of the degraded PPDX samples were performed using the differential scanning calorimeter (DSC) Q2000 (TA Instruments, USA) equipped with an autosampler, RCS90 cooling accessory, and T-zero technology. Pure Ga, In, and Zn metals (5N purity, Sigma-Aldrich) were used to calibrate the output DSC signals – temperature and heat flow. For each degraded PPDX filament, seven small pieces (3–3.5 mm length) were cut-off and inserted in parallel into a low-mass Al DSC pan. In case of highly degraded PPDX samples, the equivalent amount of the disintegrated pieces was used. The pan with the PPDX sample was then hermetically sealed – thus the measurements were effectively performed in the static air atmosphere. Overall mass of each sample was 9–13 mg (accurately determined to ± 0.01 mg). The following 6-step temperature program was applied for each sample: 1) equilibration at 25 °C; 2) heating at 5 °C/min to 150 °C; 3) 5 min isothermal annealing; 4) cooling at 5 °C/min to −30 °C; 5) 5 min isothermal annealing; 6) heating at 5 °C/min to 150 °C. To verify the reproducibility of the DSC measurements, one sample was taken from each of the 8 PPDX filaments that were always subject to identical degradation conditions (pH & degradation time).

3.4. Scanning electron microscopy (SEM)

The morphology of the sutures before degradation and after each degradation period was studied using a scanning electron microscope FlexSEM 1000 (Hitachi, Tokyo, Japan). The microscope was operated in high vacuum (approx. $1.5 \cdot 10^{-3}$ Pa) in a secondary electrons mode at acceleration voltages of 10 kV and 15 kV. Before the observation, all samples were coated with a 9 nm thick layer of gold by a sputter coater EM ACE200 (Leica Microsystems, Wetzlar, Germany) to increase their thermal and electrical conductivity.

To study the potential thinning of the sutures during the degradation, the diameters of several samples were determined from the obtained

SEM images and compared. For this purpose, the following samples were selected: a non-degraded suture, the suture degraded for 6 weeks in pH 7.4 (pH 7.4–6 W), 6 weeks in pH 3.78 (pH 3.78–6 W), and 4 weeks in pH 1.2 (pH 1.2–4 W). The diameter of each sample was measured 10 × using ImageJ 1.53k (Bethesda, MD, USA) software, and the results were averaged.

3.5. X-ray microtomography (MicroCT)

The impact of the acidic environment on the material disintegration inside the suture was inspected using an X-ray microtomograph (MicroCT). For this purpose, a microCT scanner Phoenix v|tome|x (Waygate Technologies, Hürth, Germany) was employed. The following measurement settings were applied: accelerating voltage 140 kV, current 40 μA, individual exposure time 500 ms, the total number of frames 2000 (each frame was obtained as an average of 4 images), voxel size 4 μm. A complete scan of one sample took approximately 1 h and 26 min.

3.6. Raman spectroscopy

Two spectral maps were acquired on the top surface of each measured suture sample by a Raman micro-spectrometer XploRA PLUS (Horiba, Japan) equipped with LabSpec 6 software. One of the maps consisted of wide-range overview spectra (ranging from 150 to 2100 cm^{-1}), and the other of narrow-range spectra (1550–1860 cm^{-1}). The narrow-range spectral map was designated for precise evaluation of the area under the shoulder belonging to the 1733 cm^{-1} spectral peak. The excitation laser wavelength was 785 nm, and its power was 10 mW.

To suppress the influence of sample orientation on the Raman spectra, all the suture filaments were positioned parallel to the polarization plane of the excitation laser (along the vertical axis). Excessively degraded sutures, which were already crumbling into tiny pieces, were not measured by the Raman instrument because it was not possible to accurately orient the samples in the vertical direction. To eliminate the fluorescence signal, baseline correction was made in all the spectra.

The wide-range spectra were taken in a regular grid of 6 × 6 points, spaced 20 μm in the vertical direction and 10 μm the horizontal direction. A 1200 g mm^{-1} diffraction grating and a 50 × objective were used in this case. The acquisition time for one spectrum was 40 s.

The narrow-range spectra were taken in a regular grid of 8 × 5 points, spaced 10 μm in the vertical direction and 8 μm the horizontal direction. To measure the shape of the 1733 cm^{-1} peak shoulder as precisely as possible, the spectral resolution was increased by using an 1800 g mm^{-1} diffraction grating. A higher intensity of the Raman signal was achieved by selecting a 20 × objective and setting the spectrum acquisition time to 200 s.

To evaluate the suture degradation, the shoulder of the 1733 cm^{-1} peak was found to be important [27]. Therefore, the area under this shoulder (between 1736 and 1749 cm^{-1}) normalized to the height of the 1733 cm^{-1} peak was calculated for each sample from the narrow-range spectra. At first, baseline correction was made in all the spectra to allow a relevant quantification of the 1733 cm^{-1} peak height and shoulder area. Then the shoulder areas were calculated for all the spectra of the particular suture using MATLAB R2020a software (MathWorks, Natick, MA, USA), and the results were averaged. Finally, these mean values were compared among the sutures to find their dependency on the degradation time and pH.

3.7. Mechanical properties

3.7.1. Young's modulus

In each test group, described by the degradation time and the pH of the degradation solution, (pH x – y W), we measured Young's moduli of 8 monofilament samples using ordinary tensile tests performed on an Instron 3343 Single Column Testing System (Instron, Norwood, MA, USA) with a 1 kN force transducer and Instron's flat pneumatic grips. We performed the measurements at a laboratory temperature of (22 ± 2) °C. Due to polydioxanone's natural hydrophilicity that could potentially affect the measured data, we also monitored relative humidity for extreme fluctuations to ensure that the difference between the maximum and minimum relative humidity values did not exceed 10 %. We used a standard measurement procedure that has already been reported in several studies [24,27,28,32,33]. We gathered the force-extension data, which we subsequently transformed into standard stress-strain curves using the sample filament diameter d and the original effective length of the sample L_{TE}. We performed 20 measurements of L_{TE} using the Extol 3426 caliper (Madal Bal a. s., Zlín, Czech Republic). We determined Young's modulus as the slope of the longest pseudolinear part of the stress-strain curve.

3.7.2. Tensile strength

We analyzed the tensile strength of the samples and its relation to the degradation process. To express the sample tensile strength, we used the maximum force measured before the sample rupture.

3.7.3. Shear modulus

For shear modulus and shear stiffness measurements, we used the same procedure as thoroughly described (including instructional pictures and videos) by Bezrouk et al. [24]. However, in order to suppress the influence of the measuring device, we modified the published measuring device [24]. We reduced the internal friction by choosing an appropriate bearing. We also reduced the pulley diameter, which increased the sensitivity of the force measurement while maintaining sufficient accuracy of the position measurement. Instead of an elastic rubber, we used a counterweight of approximately 20 g, which ensured a constant effect of the measuring device independent of the twist magnitude.

The measuring device was attached to the Instron 3343 equipped with a 1 kN force transducer. We performed the measurements at a laboratory temperature of (22 ± 2) °C and monitored relative humidity for extreme fluctuations, due to polydioxanone's natural hydrophilicity that could potentially affect the measured data, to ensure that the difference between the maximum and minimum relative humidity values did not exceed 10 %.

In this method, a specimen (a piece of polydioxanone filament) is

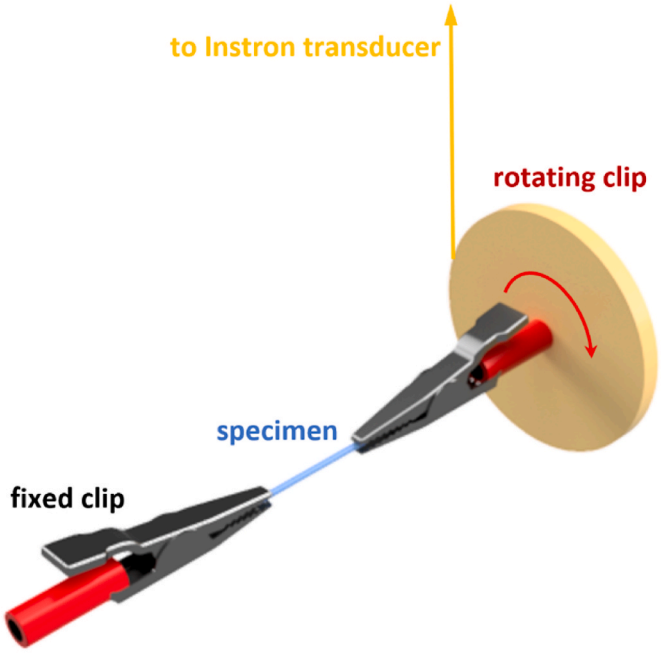

Fig. 1. The setup of the measurement device with a fixed specimen.

placed between two coaxial mini crocodile clips, fixed and twisted (Fig. 1).

From the force-extension data profile, the total system rigidity $\widetilde{K}_T$ (measurement with a specimen) and the device rigidity $\widetilde{K}_D$ (measurements taken on the device without a specimen) were determined. Then, the specimen rigidity is $\widetilde{K}_S = \widetilde{K}_T - \widetilde{K}_D$. The shear modulus of a polydioxanone filament was eventually calculated as follows:

$$G = \frac{8\overline{D}^2\overline{L}_W(\widetilde{K}_T - \widetilde{K}_D)}{\pi\overline{d}^4}$$

where $\overline{L}_W$ is the mean specimen length (20 measurements using the Extol 3426 caliper (Madal Bal a. s., Zlín, Czech Republic)), $\overline{D}$ is the mean diameter of the measuring device's pulley obtained from 20 measurements using the Extol 3426 calipers, and $\overline{d}$ is the mean stent filament diameter (20 measurements) determined using the Somet (CSN251420) micrometer screw gauge (Somet, Bílina, Czech Republic).

3.8. Statistics

The data were statistically evaluated using MATLAB R2020a software (2020, MathWorks, Natick, MA, USA) and NCSS 10 statistical software (2015, NCSS, LLC., Kaysville, UT, USA, Available online: ncss.com/software/ncss (accessed on April 21, 2023)).

Statistical comparisons of the data from mechanical tests were performed to find significant changes in relation to the degradation time and the pH of the degradation solution. We compared the data of degraded samples with the non-degraded sample data corresponding to the same specific mechanical property (i.e., Young's Modulus, Tensile Strength, Shear Modulus).

The normality of the data distribution was tested by D'Agostino omnibus test. The data from normally distributed populations with more than 10 results in a test group were described using the mean and standard deviation of the sample ($\overline{X} \pm$ SD), while the other data were described using the median and the first and the third quartiles of the sample $\widetilde{X}$ (1^{st}Q, 3^{rd}Q). Due to the limited number of samples in some test groups, we opted to use the Wilcoxon signed-rank test. To adjust for multiple comparisons and keep the familywise α at 0.05, the Bonferroni correction was used. The resulting α for a single comparison was 0.001724.

4. Results and discussion

4.1. PPDX degradation principles

The PPDX surgical sutures were exposed to aqueous media with different pHs in order to study the influence of the acidic environment on the suture degradation rate. The PPDX hydrolytic degradation/depolymerization is known [34] to proceed either via a random scission:

$$[mPPDX]_n \xrightarrow{H_2O} [mPPDX]_{n-2-x} - CH_2 - CH_2 - O - CH_2 - CO - OH + HO - CH_2 - CH_2 - O - CH_2 - CO - O - [mPPDX]_x \quad (1)$$

or via an end-chain scission, i.e., ring-closing depolymerization:

$$[mPPDX]_n \xrightarrow{H_2O} [mPPDX]_{n-1} + C_4H_6O_3 \quad (2)$$

In Eqs. (1) and (2), mPPDX is a mer unit of poly(*p*-dioxanone) PPDX:

$$[mPPDX] = -[CH_2 - CH_2 - O - CH_2 - CO - O]-$$

and $C_4H_6O_3$ is the cyclical *p*-dioxanone.

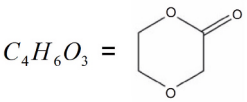

The PPDX hydrolytic degradation was reported in studies [35,36] to be strongly catalyzed by acidic media – the exact reaction mechanisms for the acid and base catalyses are described in the study by Woodard et al. [36].

In the present study, the pH of each buffer solution was unambiguously defined, as they remained unchanged during the 6-week degradation testing – see Supplementary Materials for the tabulated data. Regarding the localization of the PPDX degradation incidence, either a gradual erosion from the filament surface or a permeating reaction within the whole filament volume come into question. Note that the latter is significantly more likely for hydrophilic polymers such as PPDX.

To verify the concept of the degradation progress throughout the volume of the PPDX sutures, a basic water uptake test was performed for this sample form: ~300 mg (determined with ±0.01 mg accuracy) of dry PPDX filaments were fully immersed in distilled water for 3 h, wipe-dried from the surface moisture after removal from the water chamber, and weighed again. A consistent mass increase of ~0.6–0.8 % was observed for the PPDX filaments in this experiment (repeated 3 times with fresh sets of PPDX filaments). This unambiguously indicates that water (and by extension the H_3O^+ ions) can relatively quickly permeate inside the PPDX filaments despite the compact polymer structure associated with extrusion-based manufacturing. It is, therefore, reasonable to expect the degradation/hydrolysis to proceed within the full filaments volume.

It should be noted that the long-term filaments mass loss caused by the hydrolysis prevented us from performing days-worth experimental measurements of the water uptake – the overall mass of the long-immersed filaments decreased (compared to their initial as-purchased state) due to the PPDX dissolution even at pH = 7.

4.2. Molar mass distribution

The distribution of molar mass in the degraded PPDX samples was determined by SEC-MALS. The specific refractive index increment for PPDX was determined in the online mode assuming 100 % mass recovery; the value of $dn/dc = (0.208 \pm 0.003)$ ml/g was obtained for the non-degraded filament. The average molar masses determined for each combination of pH and degradation time were expressed as the number-average molar mass M_n, weight-average molar mass M_w, and z-average molar mass M_z.

The evolution of these three quantities with pH and degradation time is for our PPDX samples shown in Fig. 2a–c. It is immediately apparent that the dependences are very similar for all three expressions for the average molar mass, differing practically only in the Y-axis scaling. The mutual relationship between the magnitudes of the three averaged molar masses follows the commonly observed pattern $M_n < M_w < M_z$.

Regarding the actual trends observed in Fig. 2a–c, the degradation in pHs 3.78–7.4 proceeds practically linearly at the following respective rates (M_x decreases) for M_n, M_w, and M_z: (-7800 ± 300) week^{-1}, (-8700 ± 350) week^{-1}, $(-10{,}900 \pm 600)$ week^{-1}. Assuming the continuation of the degradation at similar rates, the estimated complete degradation times would be (8.2 ± 0.3) weeks, (9.2 ± 0.4) weeks, and (10.0 ± 0.5) weeks, based on the M_n, M_w, and M_z data, respectively. In the time span of the present measurements, no significant curvature of the M_x-t dependences was identified. Nonetheless, the assumption of the continuation of the linear decrease is still rather speculative because even the significantly faster degradation at lower pHs proceeded more-

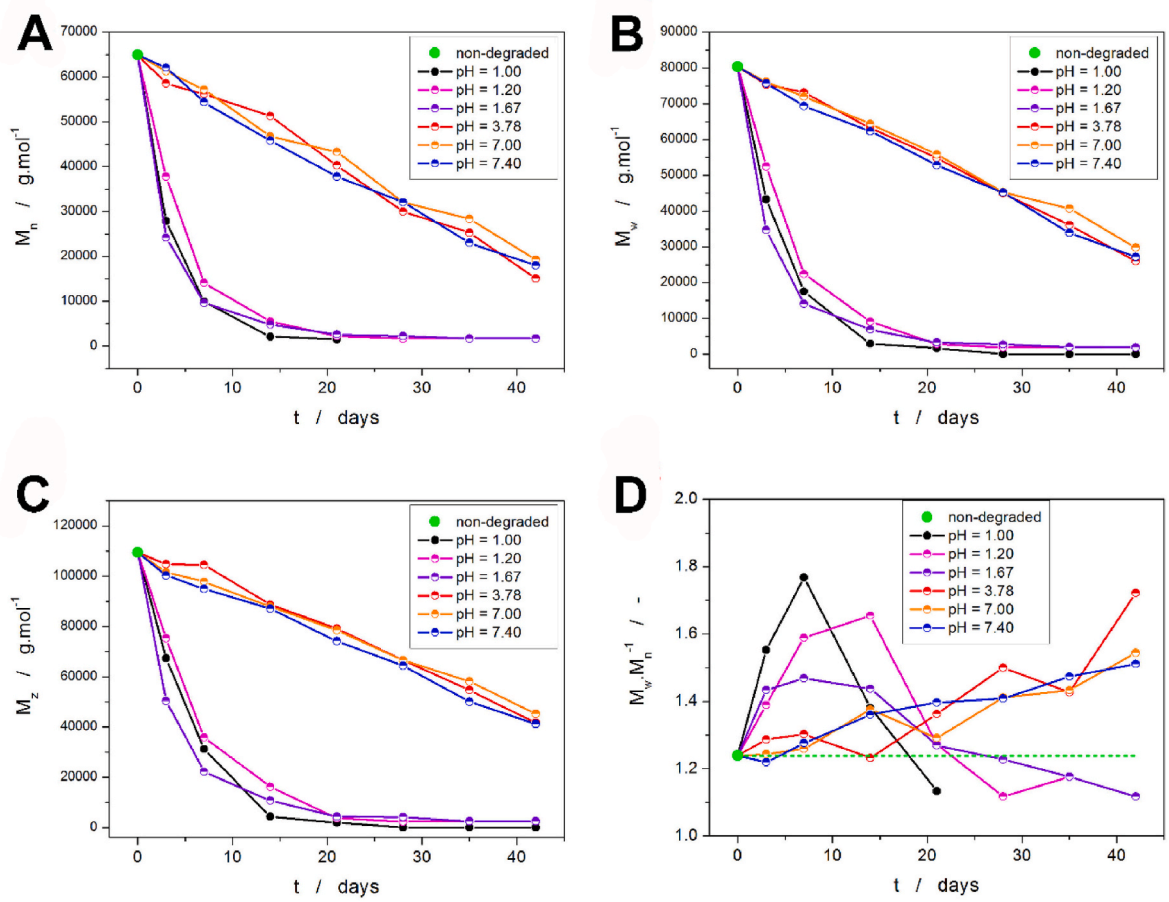

Fig. 2. (a–c) Dependences of averaged molar masses M_n, M_w, and M_z on the degradation time in different pHs. (d) Dependences of the dispersity index M_w/M_n on the degradation time in different pHs.

or-less linearly in the corresponding M_x range, and the degradation started to significantly slow down only during the last ~35 % of the full conversion process. It is, therefore, safe to say that in the 3.78–7.4 pH range, the minimum degradation time for the present PPDX sutures is 8.5–10.5 weeks.

On the other hand, the PPDX degradation in pHs 1.0–1.67 is massively accelerated, with the average molar masses decreasing to ~15 % of their original value during the first week. Full degradation of the samples then occurred within 2–3 weeks. It is, however, noteworthy that the degradation rate slowed down significantly after the first week. Interestingly, the degradation rate (especially of high molar mass polymeric chains) is the highest for pH = 1.67, which may indicate a "sweet spot" with regard to the combined influences of the surface PPDX depolymerization and the simultaneous penetration of the acidic medium inside the filament volume. At low molar masses (~10,000), the PPDX degradation in pH = 1.67 significantly slows down and is exceeded by that in pH = 1.0.

Important information can be derived also from the dispersity ($Đ$, defined as M_w/M_n), which reflects the polymer chain lengths heterogeneity – see Fig. 2d. During the initial degradation stage in pHs 1.0–1.67, the system dispersity clearly significantly increases, and returns below the initial value only momentarily before the complete sample degradation. At higher pH values (3.78–7.4), the PPDX dispersity slowly decreases during the whole 6-week period, indicating that the terminal degradation stage has not yet been reached. The distribution curves in Fig. 3 vividly describe the changes in the molar mass distribution in the course of degradation. At the end of degradation at low pH, the material consists solely of oligomeric molecules with molar masses much below 10,000 g/mol, whereas the fraction of these oligomers in the material degraded at approximately neutral pH remains below about 10 %.

It is clear from Fig. 2a–c that the pH-dependent decrease of the molar mass progresses in two distinct regimes, as revealed by the current selection of the buffers. Given the roughly linear M_w decrease in the 30,000–110,000 g mol^{-1} range within both regimes (Fig. 2b), it can be argued that a similar depolymerization mechanism is involved (despite the seemingly significantly different M_w-t profiles). Further support for this claim will be introduced in the following sections. Since pH expresses the decimal logarithm of the H_3O^+ ions concentration, the pH = 3.78 represents approximately 1 % of the concentration associated with the pH = 1.67 buffer. This gives the pH framework for future studies aimed at definitely disclosing this hypothesis.

4.3. Thermal analysis

Another experimental technique used to characterize the degraded PPDX filaments was differential scanning calorimetry. Essentially, three types of calorimetric curves were obtained as the response to the applied cyclic DSC temperature program – see Fig. 4. The first type of response (Fig. 4a) shows a behavior typical for the non-degraded samples and samples with a low degree of degradation, where a complex 2–3 step melting process occurred during the first heating (black curve). Here, the melting begins slowly at ~80 °C and starts to proceed rapidly at ~93 °C. The main endothermic melting peak manifests itself as an overlap of two liquefaction processes, which most probably correspond to the existence of two morphologically distinct types of crystallites inherent to the as-purchased PPDX filaments; the existence of the two melting peaks can be attributed to the crystalline phases formed either from the heterogeneous surface-located defects-based crystallization centers or from the volume-located homogeneous nuclei.

During the consequent cooling (blue curve in Fig. 4a), the molten

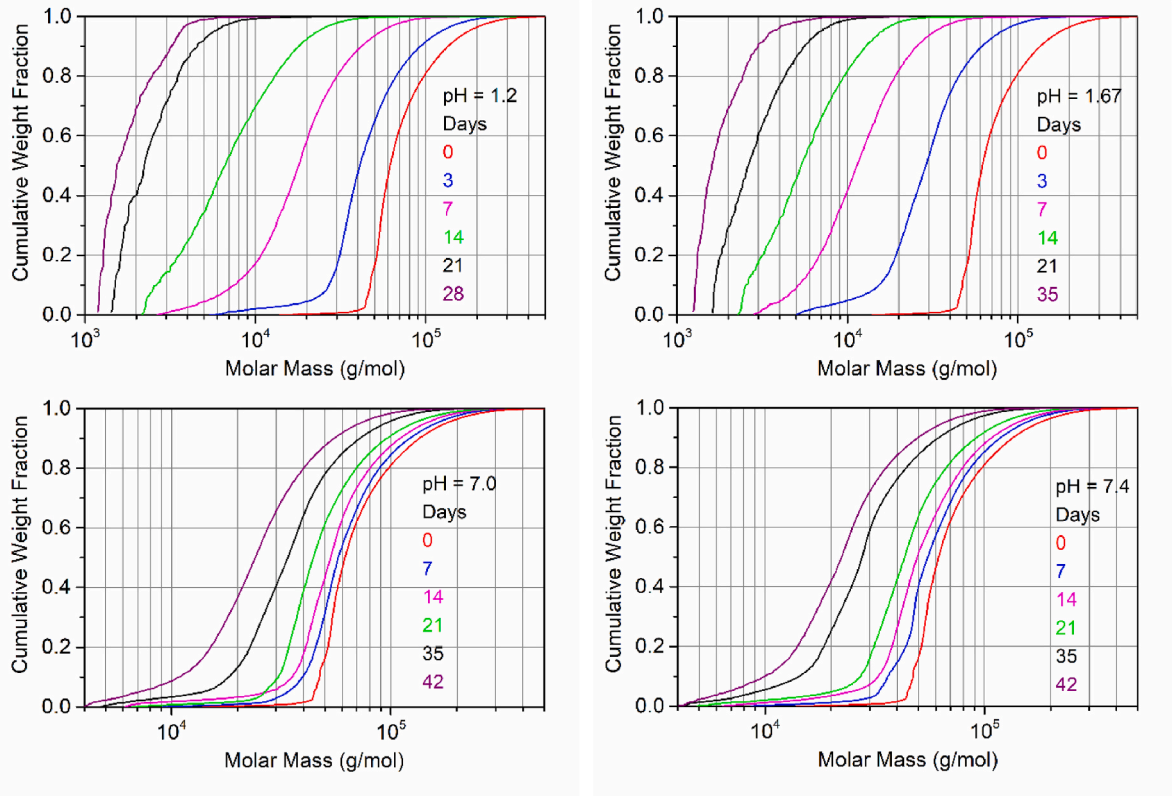

Fig. 3. Examples of the cumulative molar mass distribution curves.

PPDX material exhibits a slow partial crystallization (exothermic peak) and a glass transition (endothermic step change of heat capacity). The relatively slow partial crystallization process spread over a wide temperature range may be given by the large distribution of the molecular weights (lengths of the polymeric chains) in the non-degraded PPDX, and/or by the low amount of crystallization centers, i.e., generally slow crystal growth. At approx. −20 °C, the glass transition effect is fully manifested, indicating that the crystallization of PPDX during the cooling step is only partial and a significant portion of the amorphous phase is still present in the material.

In the consequent, second heating step (red curve in Fig. 4a), the glass transition occurs again as the first effect. At approx. 20 °C, an additional crystallization peak occurs, where another portion of the PPDX material crystallizes (note that PPDX is known to be stable as a semi-crystalline polymer [37], for which the typical crystalline content is ~45–55 %).

The occurrence of the secondary crystallization peak during the last heating step indicates that the crystal growth during the preceding cooling step was indeed too slow for the crystallizable portion of PPDX to transform fully. During further heating at approx. 72 °C, the loosened structure caused by the initial melting leads to a minor formation of additional crystalline phase. As there are no known polymorphs or competing crystalline phases for PPDX, we assume that this crystallization is simply a continuation of a previously sterically hindered/stopped growth process. Due to the initiating melting, the crystal growth process is ceased as the main portion of the PPDX material melts.

Apart from this typical example of DSC curves obtained for the lowly degraded filaments, two additional DSC profiles appeared with the progressing degree of PPDX degradation. Very rare occurrence can be attributed to the behavior displayed in Fig. 4b, which occurred only for a few combinations of the degradation time and pH. Here, the first heating shows a wider but monotonously shaped melting peak. During cooling, the crystallization occurs at a lower temperature (compared with Fig. 4a), but the exothermic peak is more pronounced and sharper. The glass transition effect already does not happen, as T_g (the glass transition temperature) has already decreased due to the polymer degradation below −30 °C, which was the low-T limit of the present temperature program for the DSC measurements.

During the second heating, a small melting peak occurs in the ~15–25 °C temperature range, which corresponds to the melting of crystallized *p*-dioxanone [38] (monomer from which PPDX is formed). The occurrence of this melting peak was very rare, and in the present study was observed only for one combination of the degradation conditions. Its presence, however, is of crucial importance for the interpretation of the changes in the DSC curves occurring with the PPDX degradation. Firstly, the very presence of a significant amount of *p*-dioxanone confirms that the hydrolytic degradation of PPDX indeed proceeds via chain-end scission, when monomers are released via the so-called unzipping or depropagation – the depolymerization mechanism is thus similar to that of thermal degradation of PPDX [39]. The presence of *p*-dioxanone also explains the marked decrease in T_g, which is caused by the plasticization effect of the monomer units on the PPDX chains. During further heating, the DSC curve exhibits features similar to those observed for the non-degraded PPDX, i.e., small additional crystallization in the close vicinity of the initiating melting. However, the melting proceeds in two distinct (but still overlapping) steps, indicating the formation of two morphologically different crystalline phases.

The third type of DSC record is shown in Fig. 4c. This behavior was typical for strongly degraded PPDX filaments. The DSC profile is practically similar to that displayed in Fig. 4b with the exception of the missing melting peak corresponding to the presence of *p*-dioxanone. Since the amount of *p*-dioxanone is continuously increasing, the disappearance of the *p*-dioxanone melting peak indicates that the *p*-dioxanone crystallizes only under specific conditions, where it is present in a relatively small amount and (possibly) still closely surrounded by the PPDX chains. In heavily degraded samples, the large amounts of monomers make the structure loosened/flexible enough for the *p*-dioxanone to flow among the crystallizing domains of PPDX and not to be

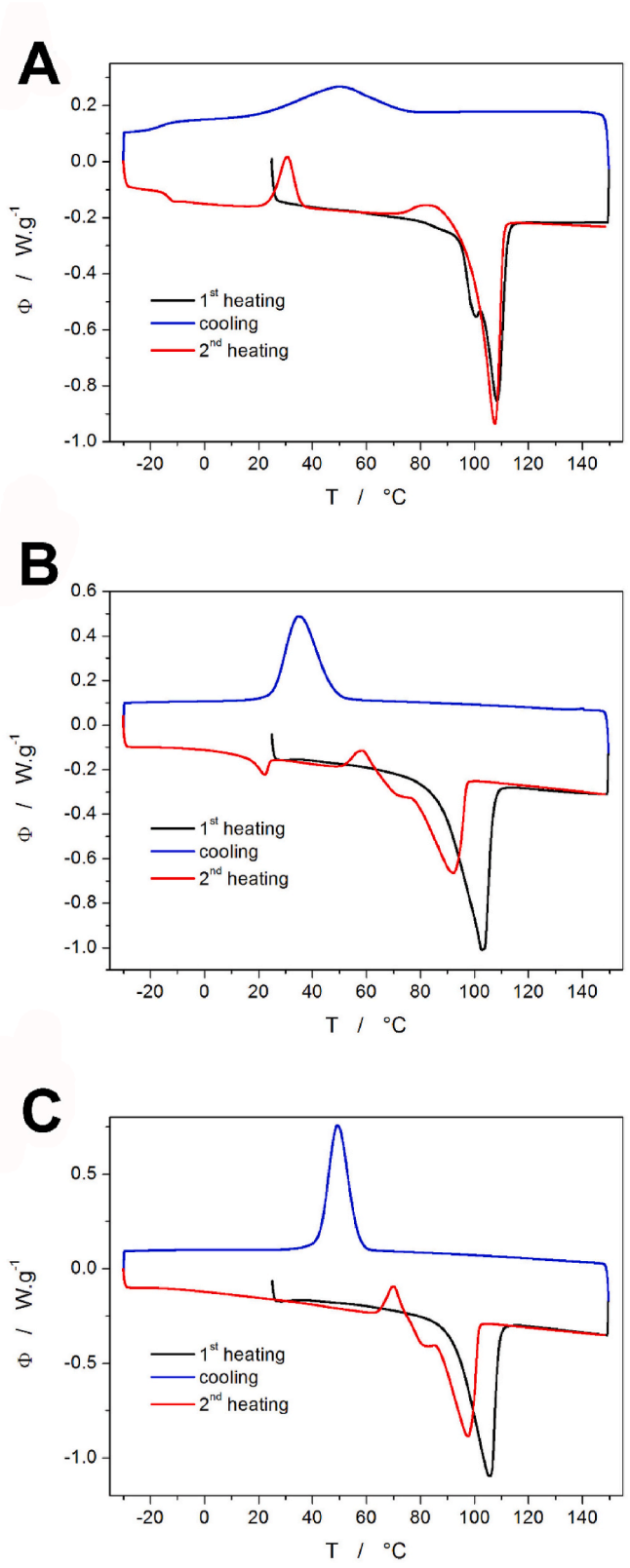

Fig. 4. Examples of three archetypal DSC cycles observed for the different degrees of PPDX degradation.

sterically forced towards crystallization by them.

The occurrence of the particular behavioral archetypes (as introduced in Fig. 4) depends on the degradation time and pH introduced in Table 1. As is apparent, the archetypal changes in the thermal behavior

Table 1
The occurrence of behavioral archetypes introduced in Fig. 4 in dependence on the degradation time and pH. The letters A, B, C correspond to the same-labeled graphs in Fig. 4.

pH	Day						
	3	7	14	21	28	35	42
1.0	A	B	C	C	C	C	C
1.2	A	A	C	B	C	C	C
1.67	A	C	C	C	C	C	C
3.78	A	A	A	A	A	A	A
7.0	A	A	A	A	A	A	A
7.4	A	A	A	A	A	A	A

during the DSC cycles occurred only for highly acidic media. Interestingly, achieving full crystallinity during the cooling step (case C) or the formation of the crystalline *p*-dioxanone (case B) are not a simple function of pH or time. The driving factors for the both phenomena are most likely the combined effects of the increase in *p*-dioxanone content (due to the degradation/depolymerization), a variability of its distribution due to the preferential degradation of the amorphous phase, and a pH-dependent decrease in molecular weights (including their distribution). The markedly increased tendency towards crystallization generally occurs in the second week of the degradation. The fact that for pH = 1.67, *p*-dioxanone crystallization was not recorded does not mean that it did not occur at all. The combination of the factors for this phenomenon appears to be very specific, and the window of its manifestation could be only a few days in between the testing intervals.

The DSC measurements of the increasingly more degraded PPDX filaments were evaluated in dependence on the degradation time and pH – see Fig. 5. Note that for pH = 1.0, the evaluation of certain quantities was largely biased by the influence of an increased water uptake that could not be properly dried in time for the timely DSC measurement. These data were not included in Fig. 5 – hence the shortened corresponding dependences in graphs in Fig. 5b–d. Starting with the evolution of T_g (Fig. 5a), it is apparent that the acidic environment highly accelerates the PPDX depolymerization (formation of *p*-dioxanone monomers) that causes a rapid decrease in T_g due to the plasticization. After 14 days of degradation, T_g of the samples degraded in pHs 1.0 and 1.67 was already below −30 °C; T_g of the sample degraded in pH = 1.2 was borderline detectable in the measured temperature range. The PPDX filaments degraded in pHs 3.78, 7.0, and 7.4 did not show significant changes in T_g.

The tendency towards crystallization (during cooling + during second heating) is for the melted PPDX samples shown in Fig. 5b. The tendency is expressed as the overall crystallization enthalpy ΔH_c (sum of the areas under the crystallization peaks recorded during the cooling and consequent heating) normalized to the corresponding enthalpy of melting measured during the second heating scan ΔH_{m2}. Note that the absolute values of the summed ΔH_c can be slightly inaccurate because DSCs cannot be calibrated on cooling (hence the value of $\Delta H_c/\Delta H_{m2} > 1$). However, the case-to-case comparison is still valid and shows slightly increased amounts of the crystalline phase being formed in the re-melted, highly degraded samples. This finding is consistent with the conclusions of the recent study by Svoboda et al. [40] on the thermal depolymerization of PPDX.

The degree of PPDX crystallinity χ_c (amount of the crystalline content) was for the degraded samples determined based on the melting enthalpies measured during the first (Fig. 5c) and second (Fig. 5d) heating. The melting enthalpy of fully crystalline PPDX was taken from the study by Ishikiriyama et al. [41]: $\Delta H_{m100\ \%} = 141.18$ J/g. The measurements performed directly on the as-degraded samples (χ_{c1}; Fig. 5c) show that in the acidic environment, the crystallinity markedly increases – up to ~85 % after 42 days of degradation. Since the formation of a new crystalline phase is ruled out under the given experimental conditions, the data in Fig. 5c unambiguously confirm that the

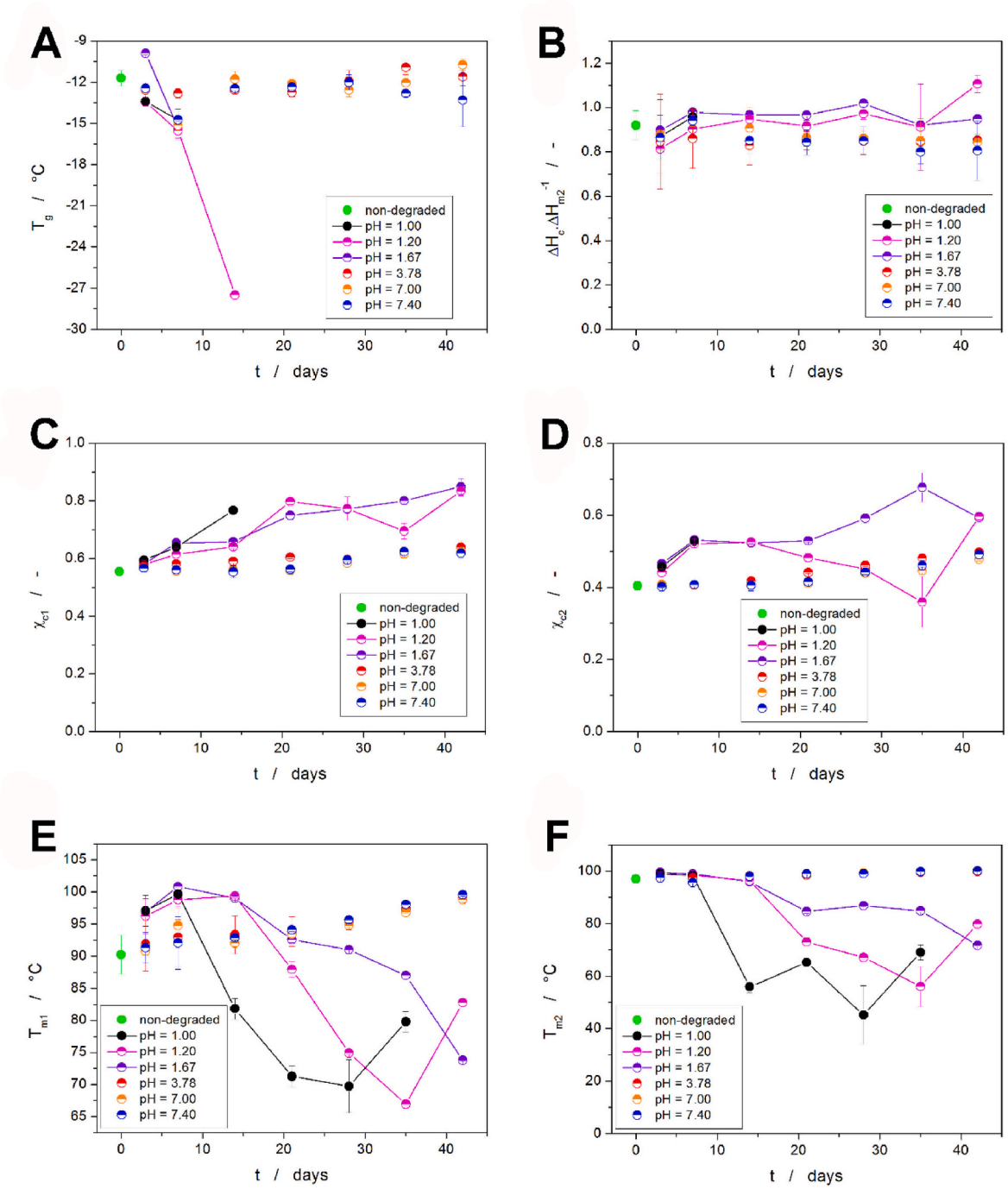

Fig. 5. Evolution of the glass transition temperature (T_g), normalized overall crystallization enthalpy ($\Delta H_c/\Delta H_{m2}$), degrees of crystallinity for the first and second heating scans (χ_1 and χ_2), and temperatures of melting for the two heating scans (T_{m1} and T_{m2}) with pH and degradation time.

amorphous phase is degraded/dissolved preferentially. A very slow (and small in magnitude) increase in χ_{c1} can also be identified for the materials degraded in pHs 3.78–7.4. Akin results were also obtained for χ_{c2} determined for the re-melted and re-crystallized PPDX during the second heating scan. These results indicate a higher tendency towards crystallization – similarly to Fig. 5b.

Particularly interesting data were obtained for the melting temperature values (see Fig. 5e and f). The non-monotonous dependence of T_{m1} on t observed for the PPDX samples degraded in highly acidic conditions can be explained by the following combination of factors: The first relatively high increase in T_{m1} is caused by the disappearance of the low-T shoulder of the main melting peak, which most probably corresponds to the melting of the surface-located crystallites – these crystallites are evidently dissolved/depolymerized significantly faster compared with the main volume/bulk-located portion of the crystalline phase. The major decrease in T_{m1} is then associated with the dominating effect of the overall decrease in molecular mass due to the rapidly proceeding depolymerization.

However, this effect progressively slows down as the molecular masses get reduced by ~1.5 orders of magnitude (see Fig. 3). The low-M_w tail of the distribution curve is fully dissolved, and the remaining portion of the PPDX crystalline phase shows much more uniform distribution of polymeric chain lengths. The progressively increasing uniformity of the crystalline phase morphology could itself account for the

increase in T_{m1} observed for the last stages of the PPDX degradation. However, one also has to bear in mind the practically ceased depolymerization in these degradation stages – as is evidenced in Fig. 3. This may indicate a prevailing influence of the competing re-polymerization reaction due to the increasing solution acidity and *p*-dioxanone concentration.

Regarding the PPDX samples degraded in the pHs 3.78–7.4, the apparent increase in T_{m1} is caused by the slow diminishing of the low-*T* shoulder of the main melting peak. Interestingly, this effect completely negates the quite significant decrease in the average molecular masses M_w – this may indicate an uneven distribution of polymeric chain lengths in the two crystalline phases corresponding to the two steps of the melting process. The evolution of trends for T_{m2} is very similar to that for T_{m1} except for the continuous increase in the melting temperature due to the diminishing low-*T* melting shoulder; the absence of this effect is shared across the pH dependences. The low-*T* shoulder does not occur after the first re-melting until high degrees of degradation. It shows that the initially uniform formation of the crystalline phase (during cooling in the DSC) is progressively more influenced by the presence of the monomer.

4.3.1. Scanning electron microscopy

SEM observations revealed that the surface of a suture before degradation is fairly smooth and without any visible damage (Fig. 6a). The subsequent degradation of the material went on similarly in all degradation solutions – from the perspective of morphological changes observable by the SEM, the degradation process can be divided into 4 successive stages.

1. The suture filament remains compact, with no surface defects visible (Fig. 6b and c).
2. The filament gets embrittled and loses its strength, which is evidenced by brittle fracture and flaking of the material (Fig. 6d–g,j), in some cases also accompanied by the emergence of curly "shavings" (Fig. 6g). Cracks oriented approximately in the direction of the filament axis can be seen too. We observed that these defects were not present on the samples immersed in the degradation solution, but they were formed after removing the samples from the solution.

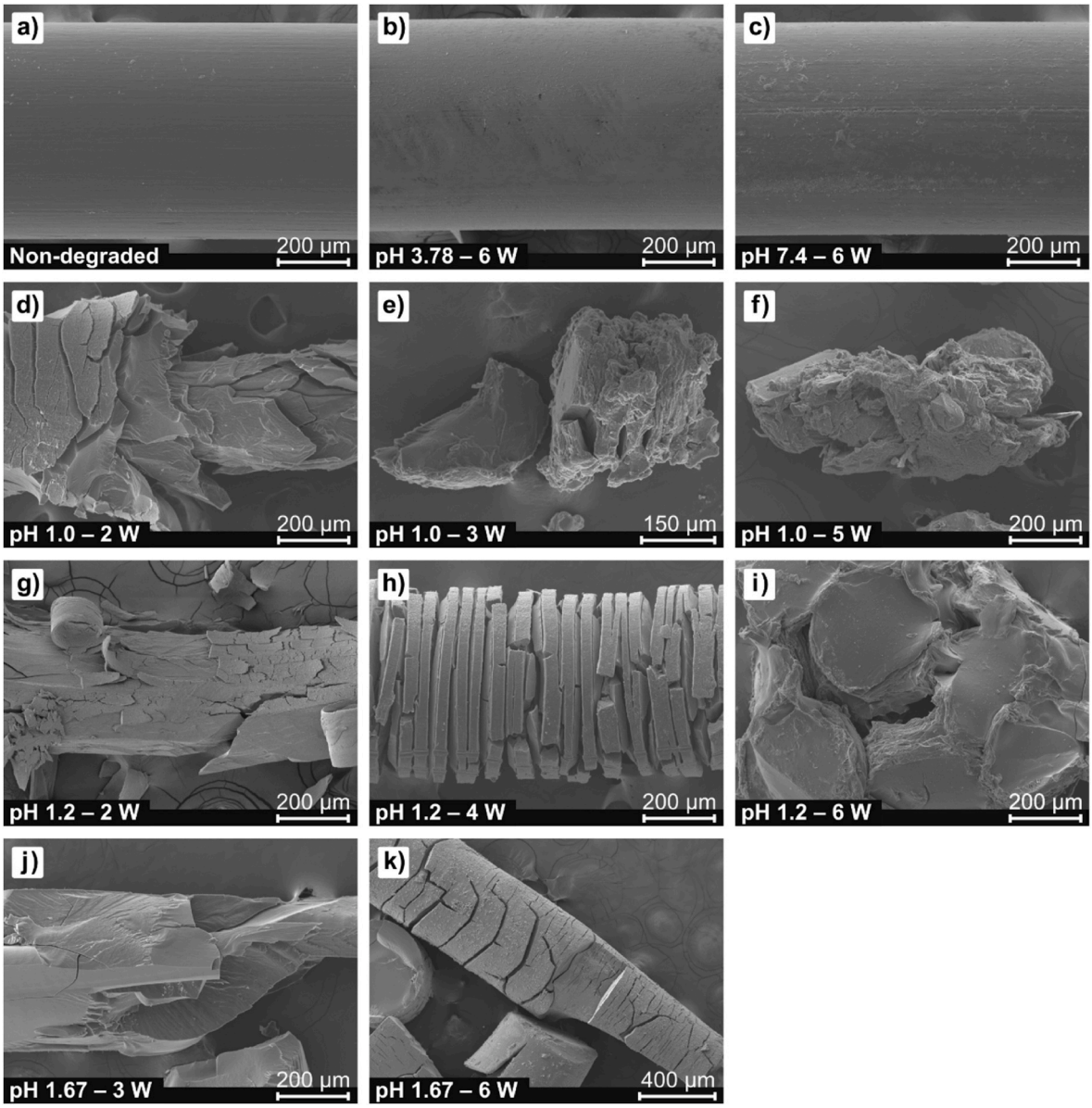

Fig. 6. Morphology of the sutures before degradation (a) and after degradation in the solutions of pH 1.0 (d, e, f), pH 1.2 (g, h, i), pH 1.67 (j, k), pH 3.78 (b), and pH 7.4 (c). W – weeks of degradation.

Formation of these defects can therefore be ascribed to the manipulation of the sample and its drying.

3. Cracks perpendicular to the filament's longitudinal axis appear (Fig. 6e–h,k). Based on the depth of these cracks, it is reasonable to assume that they were formed already during the degradation in the solution and only broadened by the sample drying. As the degradation time increases, the cracks become deeper and more open, resulting in a gradual loss of macroscopic integrity that progresses from the surface inwards.
4. The material takes the form of small glued-together lumps (Fig. 6f–i).

The rate of observable deterioration through these stages clearly depends on the pH of the solution used: lower pH values (stronger acids) result in faster degradation and vice versa.

Fig. 6d shows that in the pH 1.0 solution, flakes of the material break off from the outside region already after 2 weeks of degradation (a consequence of material brittleness). After 3 weeks, the filament crumbles into small pieces, and its surface is considerably malformed (Fig. 6e). After 5 weeks, only small lumps of irregular shape remain from the sample (Fig. 6f). Perpendicular cracks are not well visible for this pH (only a bit in Fig. 6e), likely because the structural changes for pH 1.0 are so fast that the perpendicular cracks would appear between 2 and 3 weeks of immersion.

As for the pH 1.2 solution, cracks of brittle fracture can be seen after 2 weeks of degradation (Fig. 6g). Surface curly "shavings" – probably formed by surface tension forces – are apparent here too. Fig. 6h demonstrates typical perpendicular cracks observable after 4 weeks in pH 1.2. After 6 weeks in the pH 1.2 solution, only small glued-together lumps were found (Fig. 6i), similar to those observed after 5 weeks of immersion in the pH 1.0 solution.

The degradation in the pH 1.67 solution progressed considerably slower. The 3-weeks degraded sample exhibits brittle behavior (Fig. 6j). After 6 weeks (Fig. 6k), perpendicular cracks can be seen in addition to flaking typical for a brittle fracture. However, these cracks are less developed in comparison with the sample immersed for 4 weeks in the pH 1.2 solution. Cracks like those in Fig. 6h are expected to appear after a longer period (but in this research, the maximum degradation time was 6 weeks).

The samples immersed in the solutions of pH 3.78 and pH 7.4 did not exhibit any surface cracks even after 6 weeks of degradation (Fig. 6b and c). To compare, the study by Loskot et al. [27] has shown that on a similar PPDX filament (taken from a medical stent in that case), first small cracks were formed after 8 weeks of immersion in PBS of pH 7.4. It can therefore be expected that similar structural changes will also be present on the suture filament after approx. 8 weeks in the pH 7.4 solution, all the more so in the pH 3.78 solution.

Table 2 shows the diameters of selected samples, determined from the SEM images. Based on these diameters, it is evident that some erosion of material from the suture surface occurs during the degradation process. However, the material loss is quite small: the most significant diameter reduction (about 12 %) was found for the sample after 4 weeks of degradation in pH 1.2, but this sample (Fig. 6h) was already nearly disintegrating.

Table 2
Diameters of suture filaments at different stages of degradation.

Sample	Diameter (μm)
Non-degraded	597.3 ± 0.9
pH 7.4–6 W	587.1 ± 0.8
pH 3.78–6 W	584.3 ± 0.6
pH 1.2–4 W	525.4 ± 11.8

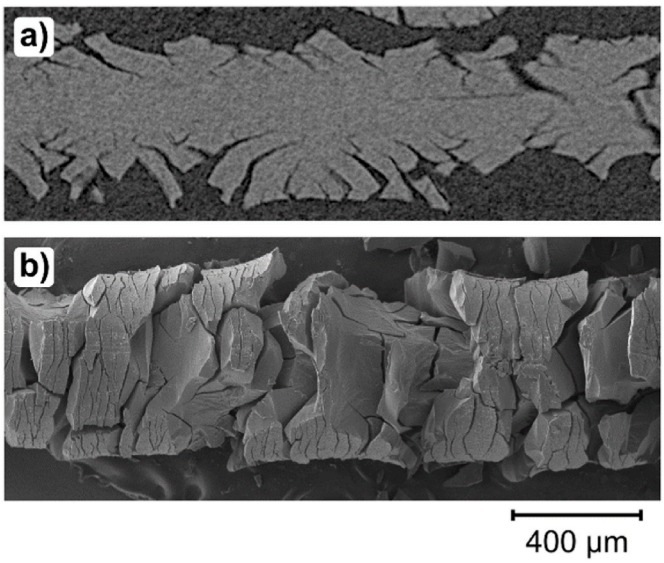

Fig. 7. A suture degraded for 3 weeks in pH 1.2: (a) cross-section imaged by microtomography, (b) outside view obtained by scanning electron microscopy.

4.4. X-ray microtomography

The MicroCT technique enabled to reveal the internal structure of sutures subjected to degradation. Fig. 7a shows a cross-section of a suture after 3 weeks of immersion in the pH 1.2 solution. In the outer region of the filament, the material is flaking off, while the central part of the filament has so far retained its integrity. This behavior gives evidence that the loss of macroscopic integrity of PPDX filaments progresses from their periphery inwards.

For comparison, an SEM image of the filament degraded under the same conditions is provided in Fig. 7b. While the SEM image better shows the fine structure of the sample topography, the arrangement of the cracks inside the filament is better visible in the MicroCT image (Fig. 7a).

Finally, the MicroCT investigations did not reveal any voids inside the bulk of the samples. This is true for both the non-degraded and variously degraded filaments.

4.5. Raman spectroscopy

All the wide-range overview Raman spectra were mutually similar and corresponded well to polydioxanone [27,28]. The differences among the wide-range spectra were small but important. The best-visible differences were caused by fluorescence. In most cases, the fluorescence of the PPDX filament was low, but some of the spectra were affected by a very high fluorescence signal. We noticed that this effect was related to the presence of the dye in the material.

Fig. 8 shows an averaged Raman spectrum of a non-degraded suture compared with a spectrum of a highly degraded suture (after 2 weeks of degradation in pH 1.2). In the "non-degraded" spectrum, the peaks at 483, 1242, 1403, 1610, and 1638 cm^{-1}, which belong to the dye [27], can be seen. On the contrary, these peaks are nearly absent in the "highly degraded" spectrum. The second difference between the "non-degraded" and the "highly degraded" spectrum consists in the shape of the peak at 1733 cm^{-1}, which was attributed to C=O stretching vibrations of the ester carbonyl group [27,28,42]. The 1733 cm^{-1} peak shoulder is substantially smaller for the degraded filament (pH 1.2 – 2W) than for the non-degraded filament.

The remaining strong peaks are typical for PPDX spectra measured on a precisely vertically oriented filament. The strongest peak at 870 cm^{-1} corresponds to C–O–C symmetric stretching vibration, the 1048 cm^{-1} peak belongs to the stretching vibration of C–C in the aliphatic

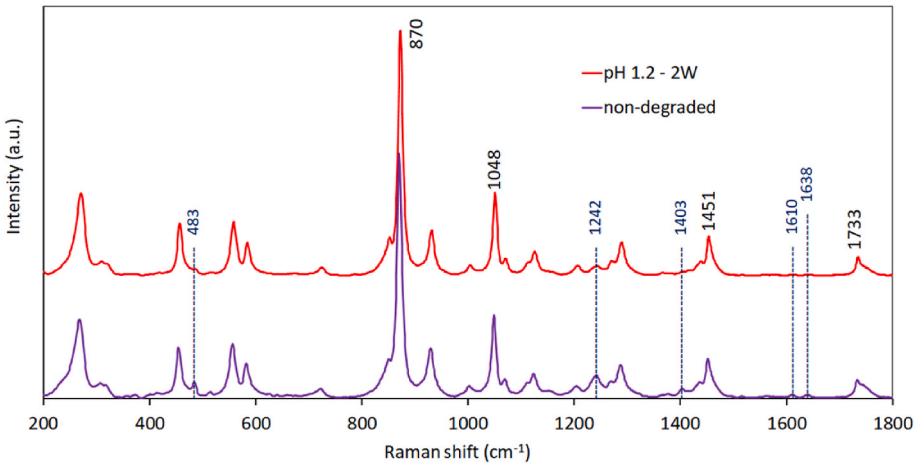

Fig. 8. Averaged overview Raman spectra (after baseline correction) of the non-degraded PPDX suture and the suture after 2 weeks of degradation in pH 1.2 (pH 1.2 – 2W).

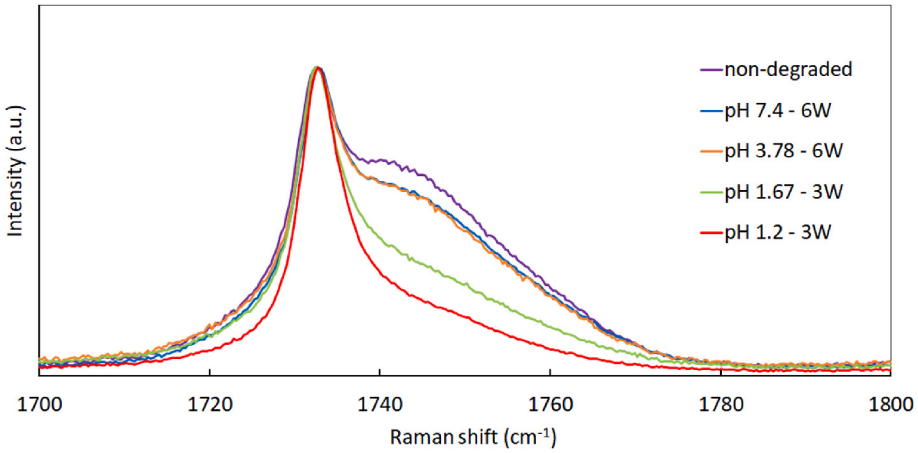

Fig. 9. The decrease of the 1733 cm^{-1} band in the narrow-range spectra of the non-degraded and four differently degraded sutures (pH 7.4 – 6W, pH 3.78 – 6W, pH 1.67 – 3W, and pH 1.2 – 3W). The Raman spectra after baseline correction were normalized and averaged.

chain, and the 1451 cm^{-1} peak was attributed to –CH2– bending [27, 42].

Fig. 9 shows a detail of the 1733 cm^{-1} peak with its shoulder. Five spectra of differently degraded PPDX (non-degraded, pH 7.4 – 6W, pH 3.78 – 6W, pH 1.67 – 3W, and pH 1.2 – 3W) are plotted in the graph. Each spectrum was obtained as an average of all the spectra from one narrow-range spectral map. The spectra of the sutures degraded for 6 weeks in pH 7.4 and pH 3.78 are almost identical in shape, and their shoulders are smaller than that of the non-degraded suture.

The shoulder in the spectrum of the sample pH 1.67 – 3W is smaller than that of the sample 1.2 – 3W, although their degradation period was the same. Both of these shoulders are also smaller than those of the

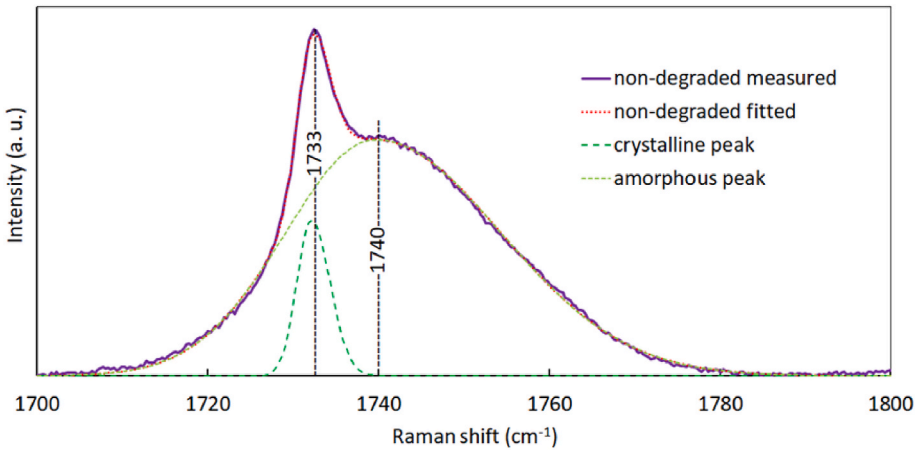

Fig. 10. Curve fitting of the 1733 cm^{-1} band in the narrow-range Raman spectrum of a non-degraded PPDX suture.

samples pH 7.4 – 6W and pH 3.78 – 6W. The exact values of the normalized shoulder areas (for all the samples) are provided in Fig. 11.

The main conclusion is that the degradation rate of a PPDX filament does not depend only on the period of degradation, but is also strongly affected by the environment's acidity. It is consistent with the conclusions of the study by Tomihata et al. [31].

In the study by Loskot et al. [27], an idea is given that the 1733 cm^{-1} band in fact consists of two peaks, which were both attributed to C=O stretching vibrations. The sharp peak (located at lower wavenumbers) arises from the vibrations of the crystalline phase, while the broader peak (located at slightly higher wavenumbers) belongs to the amorphous phase.

These two peaks were distinguished by curve fitting using LabSpec 6 software from the averaged narrow-range spectrum of the non-degraded sample. The fitting determined the positions of the model peaks: 1733 cm^{-1} for the sharp peak and 1740 cm^{-1} for the broad peak (Fig. 10). Both these model peaks have the form of a Gaussian peak. As can be seen in this figure, the fitted spectrum corresponds to the measured spectrum very well.

The positions of these peaks slightly differ from the values reported by Zheng et al. [43]. The most likely reason for this difference is that our samples were PPDX filaments composed of oriented polymer chains, while Zheng's group analyzed non-oriented polydioxanone material.

The dependences of the normalized area under the 1733 cm^{-1} peak shoulder on the degradation period and pH are shown in Fig. 11. For pH 3.78, pH 7.0, and pH 7.4, the shoulder areas decreased only a little. The time dependency of the shoulder lessening was similar for the above-mentioned values of pH. On the contrary, the decrease in the shoulder area is rapid for a highly acidic environment (pH 1.0, pH 1.2, pH 1.67 and increases with acidity. This result is in good agreement with the dependency of crystallinity on pH provided in Fig. 5c.

4.6. Mechanical properties

4.6.1. Young's modulus

The temporal evolution of the filament material elasticity, indicated by changes in Young's modulus E of the material, characterizes the force exerted by the filament on the surrounding tissue, which affects its healing process.

The determined Young's modulus of the non-degraded PPDX filament is $\widetilde{E} = 1470$ (1441, 1497) MPa, which is approximately 50 % above the previously published values for PPDX suture filaments [32,33].

The stiffness of the PPDX sutures in the degradation solutions of pH 3.78 and above is maintained during the 6 weeks of degradation (Fig. 12), which agrees with the DSC data (Section *4.3. Thermal analysis*). It seems that the maintenance of Young's modulus of PPDX in pH 3.78–7.4 may result from a relatively slow material degradation compensated by increase in the proportion of the crystalline phase in the material.

In contrast, PPDX sutures in the degradation solution of pH 1.0 show a statistically and clinically significant decrease in Young's modulus after two weeks (Fig. 12). Due to advanced degradation, only 4 samples degraded in pH 1.67 were preserved after two weeks. Therefore, it was not possible to determine the statistical significance of the decrease in Young's modulus of these samples. However, the magnitude of the Young's modulus decrease is substantial, and its clinical significance can be assumed. These results agree well with the DSC data (Section *4.3. Thermal analysis*, Fig. 5.)

4.6.2. Tensile strength

Tensile strength is an important material property closely related to the degradation process, showing the filament's resistance to disintegration. In the case of surgical sutures, this property has a fundamental clinical impact, as it expresses the filament's ability to maintain the sutured tissue and also affects the way of eliminating unnecessary sutures from the treated tissue.

Tensile strength is more sensitive to the degree of material degradation compared to the Young's and shear moduli. It is probably more affected by material integrity related to polymer chain shortening, as shown by the GPC data.

A statistically significant decrease in PPDX tensile strength was observed for the degradation solution of pH 3.78 after 4 weeks and for the solutions of pH 7.0 and 7.4 after 5 weeks of degradation (Fig. 13). This appears to be consistent with the accelerated decrease in molar mass at weeks 5 and 6 (Section *4.2. Molar mass distribution*, Fig. 2, pH 3.78–7.4). For samples degraded in the solutions of pH 1.0–1.67 statistically significant decreases in tensile strengths were already observed after three days (Fig. 13). After one week, the decrease also appears to be clinically significant. As with Young's modulus measurement, only 4 samples degraded in pH 1.67 were preserved after two weeks, which is not sufficient for a statistical analysis. Nevertheless, the observed decrease in the tensile strength is substantial, and its clinical significance can also be assumed.

4.6.3. Shear modulus

Considering major surgical suturing techniques, the effect of shear modulus on the force exerted by the suture filament on the surrounding tissue is similar to that of Young's modulus. However, taking into account the possible anisotropy in the arrangement of polymer molecules given by the manufacturing process, the temporal rate of changes in shear modulus G may differ from that of Young's modulus E. This may shorten the duration of clinically relevant forces exerted by the suture filament on the tissue compared to the situation where we would

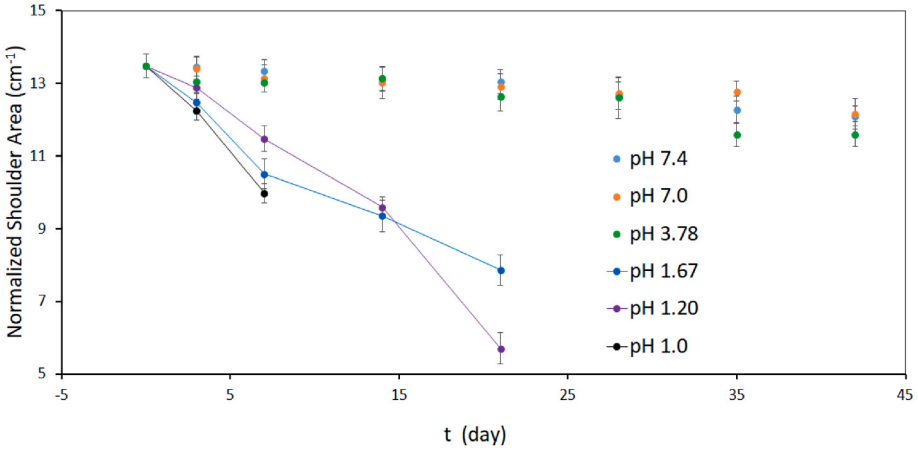

Fig. 11. A dependency of the 1733 cm^{-1} peak shoulder area on the degradation period and pH.

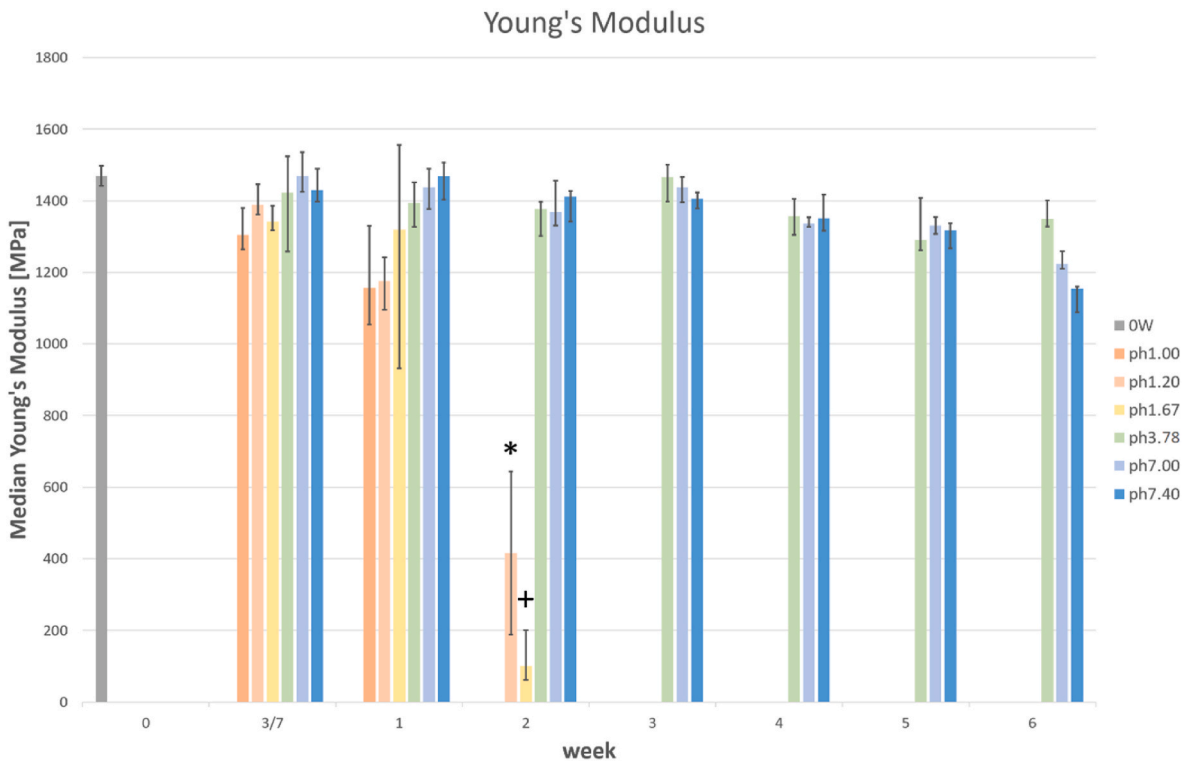

Fig. 12. Young's moduli of filaments after respective degradation periods in the degradation solution of the corresponding pH. The asterisk (*) indicates a statistically significant decrease in Young's modulus compared with the non-degraded samples (0W). The plus sign (+) indicates a substantial decrease in Young's modulus compared with the non-degraded samples (0W), which, however, could not be statistically proven.

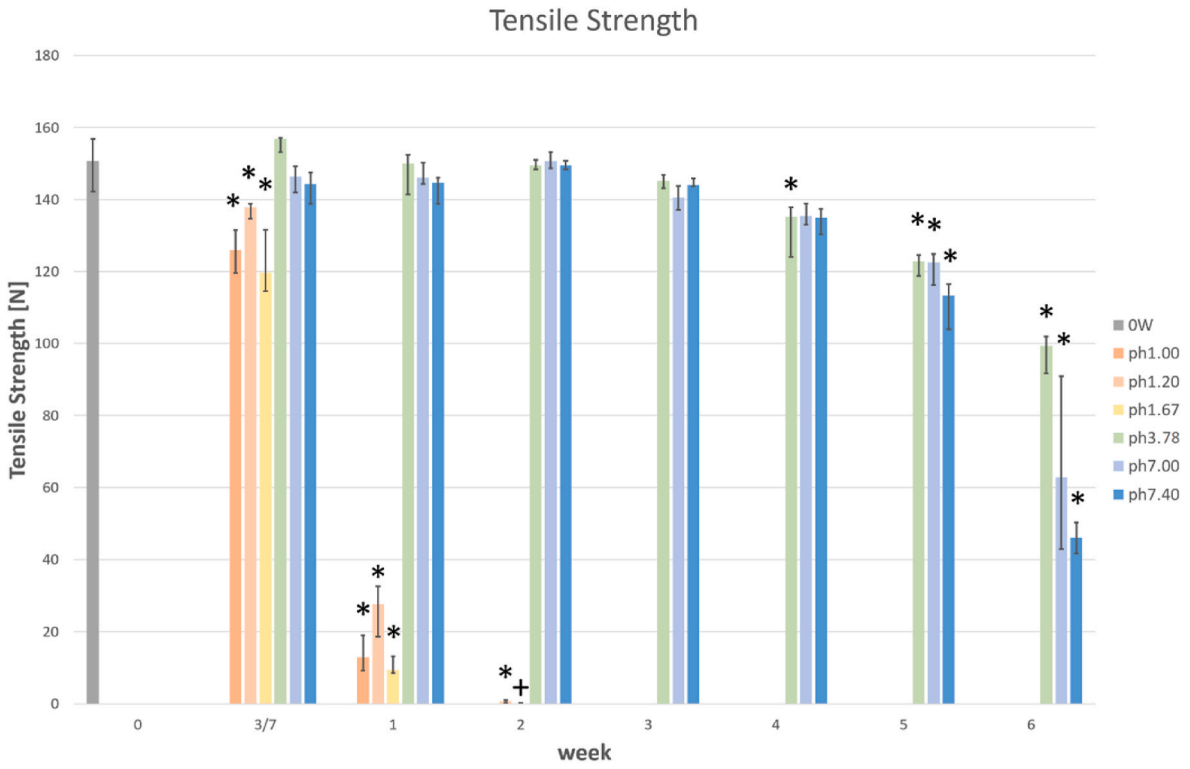

Fig. 13. Median tensile strengths of filaments after respective degradation periods in the degradation solution of the corresponding pH expressed as the maximum force measured during the test. The asterisk (*) indicates a statistically significant force decrease compared with the non-degraded samples (0W). The plus sign (+) indicates a substantial force decrease compared with the non-degraded samples (0W), which, however, could not be statistically proven.

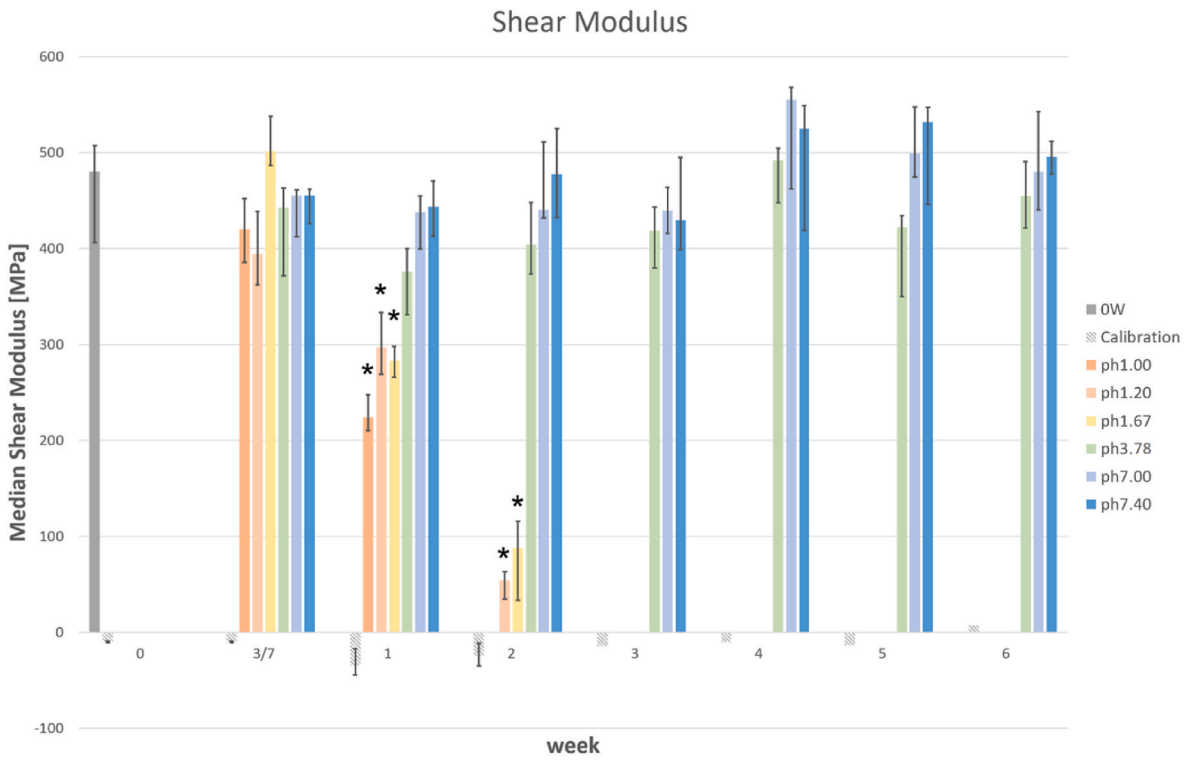

Fig. 14. Shear moduli of filaments after respective degradation periods in the degradation solution of the corresponding pH. The asterisk (*) indicates a statistically significant decrease in shear modulus compared with the non-degraded samples (0W). The Calibration denotes the influence of the measurement device expressed by a corresponding shear modulus.

consider only the temporal evolution of E.

The determined shear modulus of the non-degraded PPDX filament is $\widetilde{G} = 470\ (396, 497)$ MPa. No significant changes in shear moduli were observed for samples degraded in the solutions of pH 3.78–7.4 (Fig. 14). However, for samples degraded in the solutions of pH 1.0–1.67, there seems to be a slightly higher rate of decrease in G than that of E, and statistically significant decreases of G were observed already after one week of degradation (Fig. 14). This can be partially attributed to the inherent variability of the samples, the higher sensitivity of the improved measurement device, and the possible structural anisotropy of

Table 3
Correlations among the individual PPDX properties tested. The asterisk (*) indicates statistically significant correlations ($p < 0.003$).

	Tg [°C]	Crystalinity [%]	Mw [g.mol^{-1}]	Raman Shoulder [cm^{-1}]	Young's Modulus [MPa]	Shear Modulus [MPa]	Tensile Strength [N]
Tg [°C]		-0.252 p = 0.157	0.2395 p = 0.179	0.4217 p = 0.015	0.2602 p = 0.143	0.6456 * p < 0.001	0.4821 p = 0.005
Crystalinity [%]	-0.252 p = 0.157		-0.8591 * p < 0.001	-0.9540 * p < 0.001	-0.6570 * p < 0.001	-0.5715 * p < 0.001	-0.8355 * p < 0.001
Mw [g.mol^{-1}]	0.2395 p = 0.179	-0.8591 * p < 0.001		0.8438 * p < 0.001	0.6864 * p < 0.001	0.5544 * p < 0.001	0.8618 * p < 0.001
Raman Shoulder [cm^{-1}]	0.4217 p = 0.015	-0.9540 * p < 0.001	0.8438 * p < 0.001		0.8308 * p < 0.001	0.8205 * p < 0.001	0.9423 * p < 0.001
Young's Modulus [MPa]	0.2602 p = 0.143	-0.6570 * p < 0.001	0.6864 * p < 0.001	0.8308 * p < 0.001		0.8078 * p < 0.001	0.7671 * p < 0.001
Shear Modulus [MPa]	0.6456 * p < 0.001	-0.5715 * p < 0.001	0.5544 * p < 0.001	0.8205 * p < 0.001	0.8078 * p < 0.001		0.7716 * p < 0.001
Tensile Strength [N]	0.4821 p = 0.005	-0.8355 * p < 0.001	0.8618 * p < 0.001	0.9423 * p < 0.001	0.7671 * p < 0.001	0.7716 * p < 0.001	

Pearson's correlation coefficient	Correlation
0.00 - 0.19	very weak
0.20 - 0.39	weak
0.40 - 0.59	moderate
0.60 - 0.79	strong
0.80 - 1.00	very strong

PPDX filaments originating from the manufacturing processes, as suggested by the SEM and MicroCT results (Section 4.5. *X-ray microtomography*).

4.7. Correlations

4.7.1. Correlations – analyses

Regarding simple linear correlations (Table 3), some strong and very strong correlations can be found among the PPDX properties tested. Nevertheless, further detailed analysis revealed more complex data relationships and discovered that some – even strong and statistically significant – correlations are false positive.

For example, all correlations with T_g were found to be false positive, including the strong and statistically significant correlation between T_g and the shear modulus. Fig. 15 shows that there is probably no relationship between T_g and the shear modulus. This apparently suggests that the plasticization process does not affect these mechanical properties of PPDX in any way – at least in the stages when it was still possible to macroscopically test Young's modulus (YM), the shear modulus (SM), and the tensile strength (TS). At least given the variance of the data (Fig. 15), the correlation between T_g and the shear modulus cannot be proven, and the value of the Pearson coefficient (Table 3) is probably a matter of coincidence. Thus, it seems that the plasticization of PPDX does not significantly influence any concurrently measured mechanical property (YM, SM, TS) of the PPDX suture up to the stage of its fragmentation and the loss of its therapeutic function, as its possible influence on these properties is largely exceeded by the effect of decreasing M_w.

On the other hand, some other correlations proved to be more complex and even stronger after more detailed data analyses.

Nevertheless, it should be also noted that the correlation values listed in Table 3 express only the direct correlations between the pairs of the individual quantities. The physico-chemical background behind these values could be more complicated, *e.g.*, if multiple monitored factors were mutually correlated and/or a mutually common fundamental quantity was not identified. The exact identification, clarification and possible confirmation of the individual processes behind the respective correlations should be further investigated.

Young's modulus is very strongly correlated (R = 0.8861) with M_w down to 15,000 g/mol (blue data series, Fig. 16). Subsequently, Young's modulus decreases sharply (red data series, Fig. 16), however, the very strong correlation with M_w (R = 0.9988) may be coincidental due to the small number of data points.

This finding is consistent with a model for hydrolytic degradation of aliphatic polyesters adapted for semicrystalline polymers [44]. This model assumes that a part of the polymer chains in the amorphous phase connects the microcrystals of the crystalline phase, and degradation takes place only in the amorphous phase. The result of the model is that the decrease in Young's modulus is delayed compared to the decrease in molecular weight caused by degradation.

The relatively sudden collapse of the macroscopic structure (red data series, Fig. 16) is probably due to a joint interplay of the above-mentioned phenomena [44] with the process of polymer chains shortening. The polymer chains are mainly oriented longitudinally due to the production process of the suture fiber, leading to a loss of their entanglement, which, below a certain threshold limit, may result in the loss of the longitudinal stiffness.

Unlike Young's modulus, the shear modulus is independent of M_w down to 30,000 g/mol (blue data series, Fig. 17). Then, the shear modulus substantially decreases (red data series, Fig. 17) in a strong correlation (R = 0.9535) with M_w. It can be assumed that, as a result of the gradual loosening of the polymer structure, there is a change in the orientation of PPDX microcrystals (which is probably manifested in Raman measurements and will be discussed further), a disruption of transverse bonds in the filament material, and probably also an appearance of internal material defects (microcracks, dislocations, …). This reduces the material rigidity and integrity in the transverse direction, being manifested by a decrease in shear modulus and tensile strength. Young's modulus decreases only slightly down to M_w = 15,000 g/mol (blue data series, Fig. 16).

The tensile strength of the PPDX filament is very likely affected by the simultaneous action of phenomena causing the decrease in Young's modulus and the shear modulus. This assumption is supported by significant and strong correlations between the tensile strength and Young's modulus, and the tensile strength and shear modulus (Table 3). In the first stage of degradation, down to M_w = 30,000 g/mol (blue data series, Fig. 18), the tensile strength slightly decreases, strongly correlated with M_w in much the same way as Young's modulus (blue data series, Fig. 16). Then the tensile strength decrease suddenly accelerates (red data series, Fig. 18), following the substantial decrease in shear modulus (red data series, Fig. 17), eventually decreasing to immeasurably small values at M_w = 15,000 g/mol and less.

Crystallinity is strongly correlated with molecular weight across almost the entire range of M_w (blue data series, Fig. 19). The only

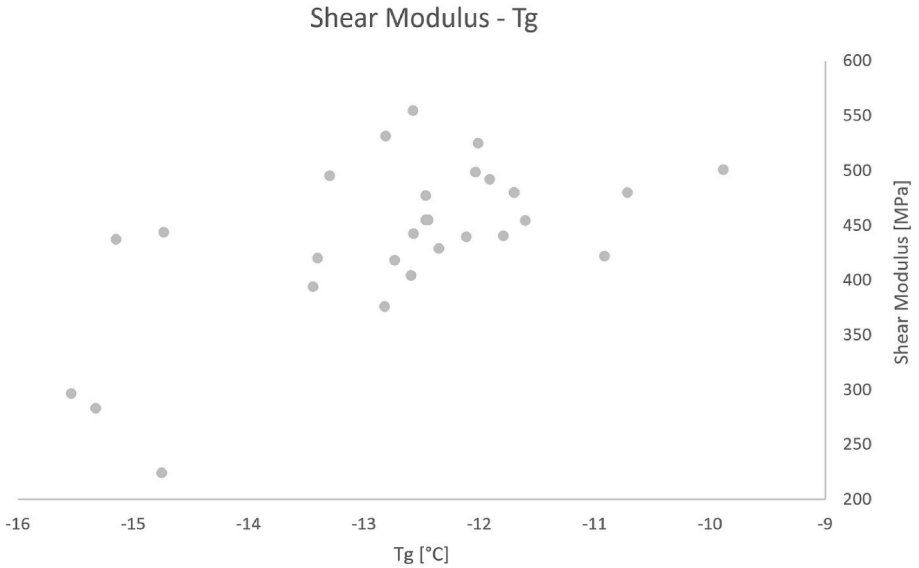

Fig. 15. Correlations between the shear modulus and T_g of PPDX.

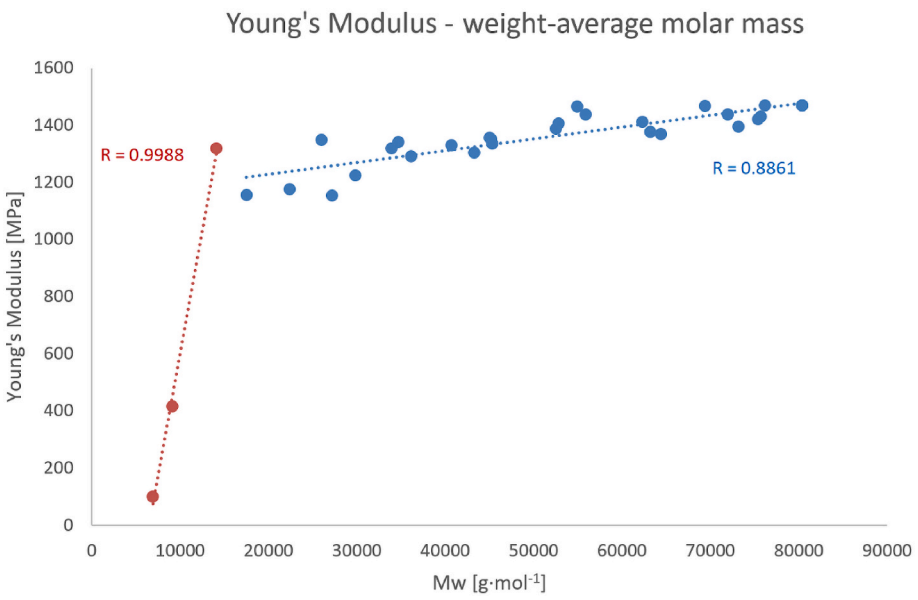

Fig. 16. Correlations between Young's modulus and the weight-average molar mass of PPDX for two separate data groups – the data with M_w below 15,000 g/mol (red) and above (blue) with the corresponding Pearson's correlation coefficients. (For interpretation of the references to color in this figure legend, the reader is referred to the Web version of this article.)

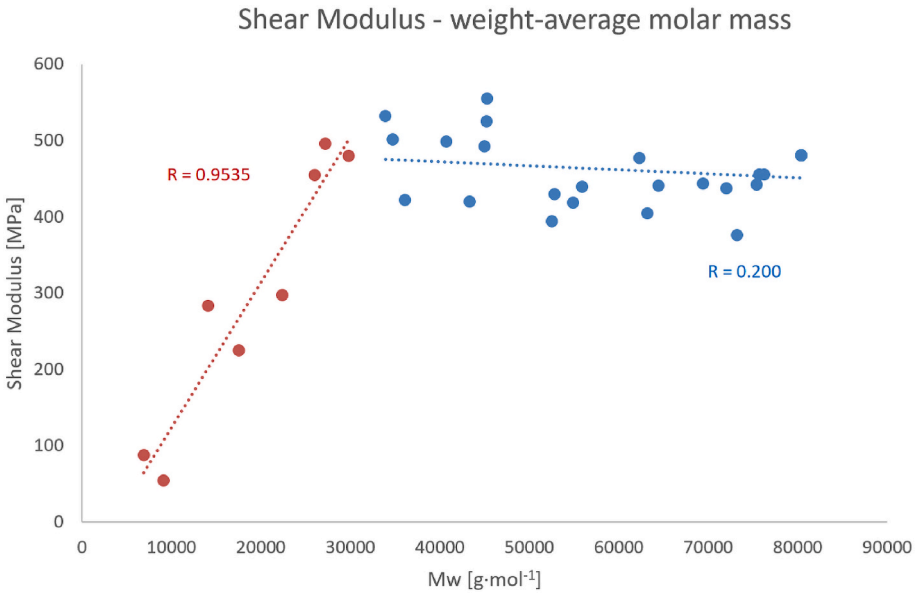

Fig. 17. Correlations between the shear modulus and molecular weight of PPDX for two separate data groups – the data with M_w below 30,000 g/mol (red) and above (blue) with the corresponding Pearson's correlation coefficients. (For interpretation of the references to color in this figure legend, the reader is referred to the Web version of this article.)

exception are the data with M_w below 6000 g/mol (red data series, Fig. 19). Thus, crystallinity seems to be a very good predictor of PPDX degradation at least until the PPDX filament substantial disintegration.

The steep increase in crystallinity (red data series, Fig. 19) may correspond to a macro-structural threshold, where either the preferentially degraded PPDX chains from the amorphous phase become short enough to penetrate through the bulk material, or the overall structure of the filament becomes porous enough for larger amorphous domains to be released from the bulk material. Either way, the amorphous phase gets preferentially released into the surrounding medium, artificially increasing the crystallinity in the remainder of the filament.

Surprisingly, unlike crystallinity (Fig. 19), the correlation between the Raman shoulder and molecular weight (Fig. 20) is not linear. Instead, there is a break in the correlation between these quantities around M_w = 30,000 g/mol, just as in the case of shear modulus or tensile strength. Nevertheless, both the correlation above M_w = 30,000 g/mol (blue data series, Fig. 20) and the correlation below M_w = 30,000 g/mol (red data series, Fig. 20) are very strong. It suggests that there is another process affecting the results of the Raman shoulder measurements.

A possible explanation arises from the principle of the polarization-dependent Raman measurement: The samples were oriented so as to achieve the minimum signal from the PPDX crystalline phase, so the relative intensity of the signal from the amorphous phase increased. Therefore, if the degradation process leads to the considered loosening of the PPDX structure and gradual loss of the microcrystals' orientation,

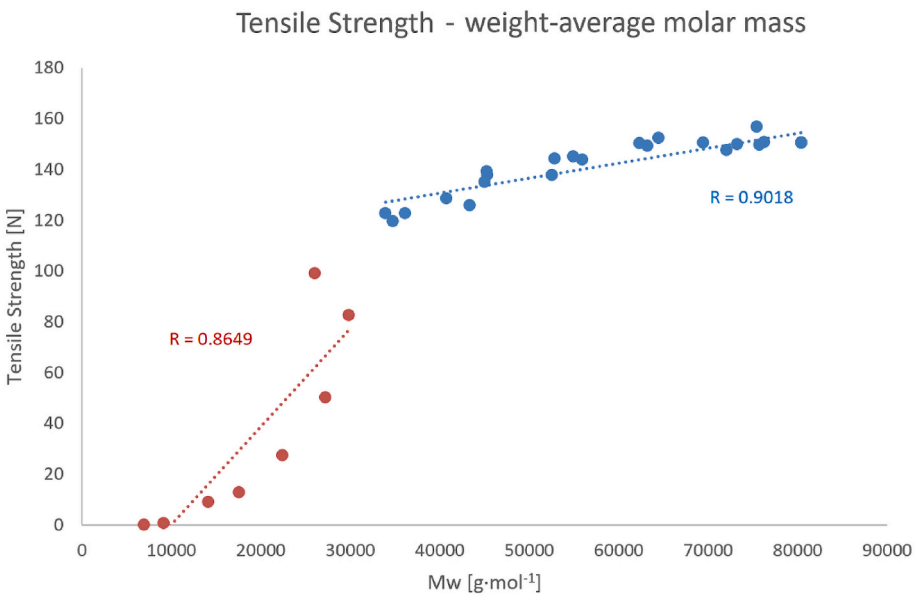

Fig. 18. Correlations between the tensile strength and weight-average molar mass of PPDX for two separate data groups – the data with M_w below 30,000 g/mol (red) and above (blue) with the corresponding Pearson's correlation coefficients. (For interpretation of the references to color in this figure legend, the reader is referred to the Web version of this article.)

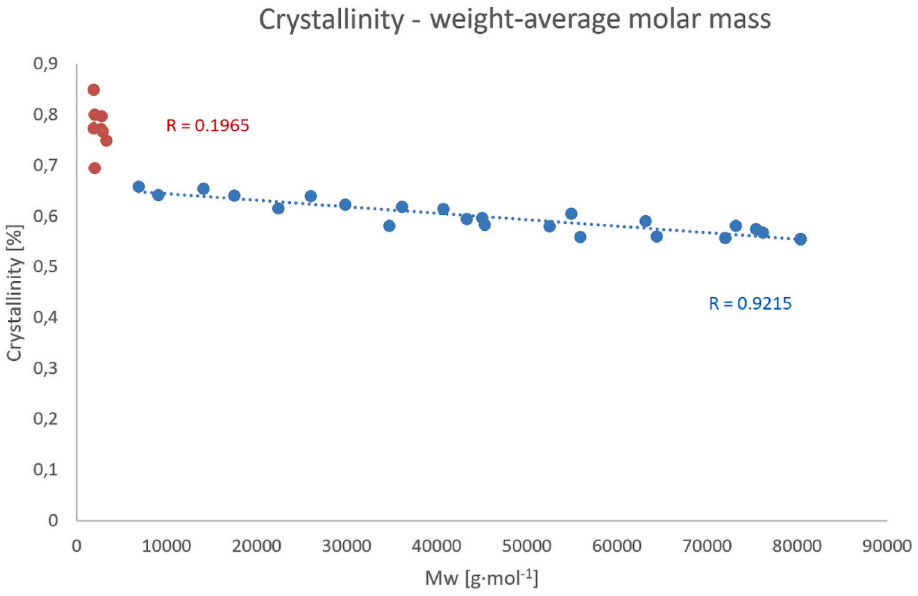

Fig. 19. Correlations between the crystallinity and weight-average molar mass of PPDX for two separate data groups – the data with M_w below 6000 g/mol (red) and above (blue) with the corresponding Pearson's correlation coefficients. (For interpretation of the references to color in this figure legend, the reader is referred to the Web version of this article.)

the level of the minimum achievable signal from the PPDX crystalline phase increases, which leads to an overestimation of its relative intensity compared to the signal from the amorphous phase.

Thus, Raman measurements carried out without further adjustments or compensations inevitably overestimate the crystallinity of the investigated PPDX. On the other hand, the Raman measurement is qualitatively more valuable than the measurement of crystallinity using DSC or molecular weight measurement, because it also contains information about changes in the arrangement of the material internal structure and the increase/decrease in its entropy. Therefore, Raman spectroscopy describes the process of degradation of PPDX suture mechanical properties better than crystallinity measurements using DSC or molecular weight measurements. This claim is supported by the stronger correlations of the measured mechanical properties with Raman spectroscopy results (Table 3). With the help of suitable compensation techniques, the crystals' arrangement information could be extracted. The values of crystallinity obtained from the Raman shoulder measurements could be determined more precisely, too.

4.7.2. Correlations and the effect of degradation rate

It should be noted that all the correlation data are an "even" mixture of low and advanced degradation for all environments from the most acidic (pH 1.0) to neutral (pH 7.4). This suggests that the degradation processes follow the same mechanism independent of the environment acidity, only at different rates: the lower the pH, the faster the degradation process.

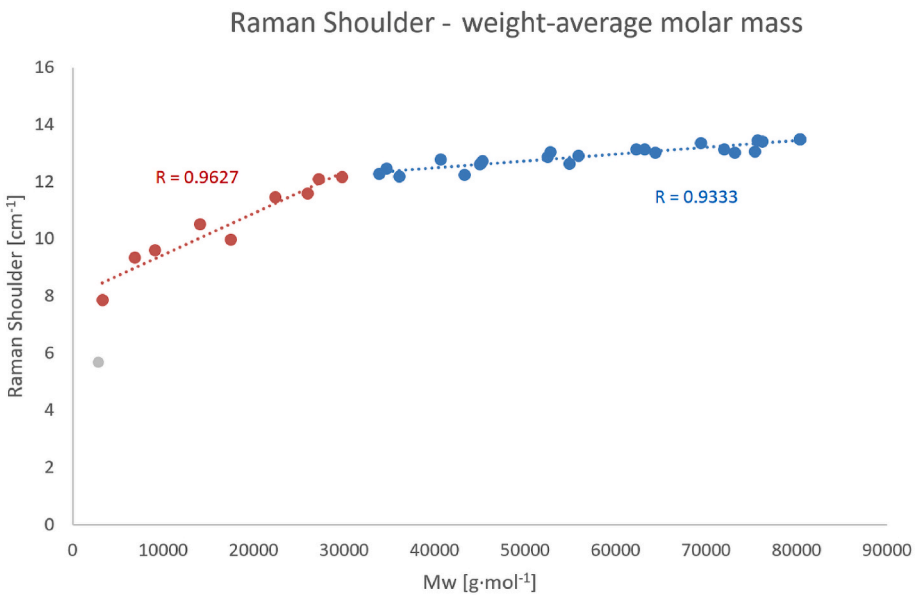

Fig. 20. Correlations between the Raman shoulder area and the weight-average molar mass of PPDX for two separate data groups – the data with Mw below 30,000 g/mol (red) and above (blue) with the corresponding Pearson's correlation coefficients. The grey color denotes possible outliers. (For interpretation of the references to color in this figure legend, the reader is referred to the Web version of this article.)

4.7.3. Correlations and their impact on theoretical models

To the best of our knowledge, there are no models for hydrolytic degradation of aliphatic polyesters describing the changes in shear modulus. However, our measurements have proven that the processes influencing changes in the shear modulus (Fig. 17) are not completely identical to the processes influencing changes in Young's modulus (Fig. 16). The shear modulus also significantly affects the material strength (see, for example, the strong correlation between the shear modulus and tensile strength – Table 3) as a key mechanical property of the PPDX suture. Therefore, it cannot be assumed a priori that Poisson's number is constant during PPDX degradation and that the shear modulus in the model can be determined by a simple conversion from Young's modulus.

As indicated by our results – such as the correlation between shear modulus and M_w, tensile strength and M_w, and Raman shoulder and M_w – the idea of gradual transverse bond disruption and the loss of order in the structure of the PPDX suture material should be included in theoretical models. Nevertheless, the shear modulus should definitely be tested separately.

5. Conclusions

The degradation of PPDX in an acidic environment is significantly accelerated. This acceleration occurs at the acidic pH = 1.67 and below. At pH = 3.0 and above, the degradation rate of PPDX is very similar to that in PBS. Determining the exact pH limit would require further research. Accelerated degradation of PPDX in a very acidic environment can be seen, *e.g.*, in stomach treatment.

From the correlation curves, where different degradation times and different acidic environments are combined, it seems that the actual degradation mechanisms do not depend on pH.

Most correlations with molar mass show a break. However, these breaks occur at different values of M_w, depending on the particular property. It can be assumed that these breaks are caused by different degradation mechanisms. One of the possible mechanisms is the loss of the original orientation of the molecules and microcrystals in the PPDX suture. The structural disorders manifest themself as visible breaks in correlations with Raman data. This suggests the need to develop a suitable compensation technique for Raman measurements.

An important conclusion arises from the position of the break in the correlation between M_w and Young's modulus (YM, Fig. 16), shear modulus (SM, Fig. 17), tensile strength (TS, Fig. 18), crystallinity (CR, Fig. 19), and normalized Raman shoulder area (RA, Fig. 20). As the breakage of the initial linear correlation gets closer to the $M_w = 0$ limit, the respective property becomes better suited for the characterization of the overall depolymerization process (that is ultimately defined by M_w, which is, however, rather tedious to obtain with sufficient accuracy). From this methodological point of view, the length of the interval of correlation with M_w, and thus the suitability of the particular quantities to characterize the polymer degradation, increases in the following order: TS ≈ SM ≈ RA < YM < CR.

The benefits of these quantities can also be perceived from the opposite perspective, i.e., based on their correlation with the loss of functionality of the bio-degrading surgical suture. Here, the baseline is given by the sudden large decrease in the tensile strength (occurring at $M_w \sim 30{,}000$), which directly corresponds to the loss of the filament's macroscopic integrity. Accordingly, the suitability of the relevant quantities increases in the following order: CR < YM < SM ≈ RA (≈TS). Raman spectroscopy is of particular interest in this regard, due to its rapidity and practically no requirements on the sample preparation or form.

Data availability

The data that support the findings of this study are available from the corresponding author upon reasonable request.

CRediT authorship contribution statement

Krisztina Dodzi Lelkes: Writing – review & editing, Writing – original draft, Visualization, Investigation, Data curation, Conceptualization. **Daniel Jezbera:** Writing – review & editing, Writing – original draft, Visualization, Validation, Resources, Methodology, Investigation, Funding acquisition, Formal analysis, Data curation, Conceptualization. **Roman Svoboda:** Writing – review & editing, Writing – original draft, Visualization, Validation, Methodology, Investigation, Formal analysis, Data curation, Conceptualization. **Štěpán Podzimek:** Writing – review & editing, Writing – original draft, Visualization, Validation, Methodology, Investigation, Formal analysis, Data curation. **Jan Loskot:** Writing – review & editing, Writing – original draft, Visualization,

Validation, Methodology, Investigation, Formal analysis, Data curation, Conceptualization. **Martina Nalezinková:** Writing – review & editing, Writing – original draft, Validation, Methodology, Investigation, Formal analysis, Data curation. **Petr Voda:** Writing – review & editing, Methodology, Investigation, Formal analysis, Data curation. **Piotr Duda:** Writing – review & editing, Visualization, Methodology, Investigation, Formal analysis, Data curation. **Alena Myslivcová Fučíková:** Writing – review & editing, Validation, Methodology, Investigation. **Tomáš Hosszú:** Writing – review & editing, Writing – original draft, Validation. **Dino Alferi:** Writing – review & editing, Writing – original draft, Investigation. **Aleš Bezrouk:** Writing – review & editing, Writing – original draft, Visualization, Validation, Supervision, Project administration, Methodology, Investigation, Formal analysis, Data curation, Conceptualization.

Declaration of competing interest

Polydioxanone (PPDX) has gained significant attention as a biocompatible and absorbable polymer used in various medical applications, such as sutures and tissue scaffolds. One of the most aggressive environments in which PPDX appliances are used is the stomach, esophagus, and some parts of gastrointestinal tract, mainly due to the very low pH. However, the effect of clinically relevant low pH on the PPDX material has not yet been investigated in detail, and the underlying degradation processes at low pH have not yet been known. Our study showed that pH in the range of 3.78–7.40 does not accelerate the PPDX degradation. Thus, with the help of suitable medication increasing the environmental pH is possible to reach the desired treatment outcome. Our study also showed a link between the change in the microcrystalline structure arrangement of PPDX during degradation and the change in the key macroscopic properties of the material.

Data availability

Data will be made available on request.

Acknowledgements

This research was financially supported by the Ministry of Youth, Education and Sports of the Czech Republic the Excelence project PřF UHK 2215/2022-2023.

Appendix A. Supplementary data

Supplementary data to this article can be found online at https://doi.org/10.1016/j.polymertesting.2024.108536.

References

[1] J.A. Ray, N. Doddi, D. Regula, J.A. Williams, A. Melveger, Polydioxanone (PDS), a novel monofilament synthetic absorbable suture, Surg. Gynecol. Obstet. 153 (1981) 497–507.

[2] G. Mauri, C. Michelozzi, F. Melchiorre, D. Poretti, V. Pedicini, M. Salvetti, E. Criado, J. Falcò Fages, M. De Gregorio, A. Laborda, et al., Benign biliary strictures refractory to standard bilioplasty treated using polydoxanone biodegradable biliary stents: retrospective multicentric data analysis on 107 patients, Eur. Radiol. 26 (2016) 4057–4063, https://doi.org/10.1007/s00330-016-4278-6.

[3] A. Siiki, J. Sand, J. Laukkarinen, A systematic review of biodegradable biliary stents: promising biocompatibility without stent removal, Eur. J. Gastroenterol. Hepatol. 30 (2018) 813–818, https://doi.org/10.1097/meg.0000000000001167.

[4] M.E. Giménez, M. Palermo, E. Houghton, P. Acquafresca, C. Finger, J.M. Verde, J. C. Cúneo, Biodegradable biliary stents: a new approach for the management of hepaticojejunostomy strictures following bile duct injury. Prospective study, Arquivos brasileiros de cirurgia digestiva : ABCD = Brazilian archives of digestive surgery 29 (2016) 112–116, https://doi.org/10.1590/0102-6720201600020012.

[5] M. Battistel, M. Senzolo, A. Ferrarese, A. Lupi, U. Cillo, P. Boccagni, G. Zanus, R. Stramare, E. Quaia, P. Burra, et al., Biodegradable biliary stents for percutaneous treatment of post-liver transplantation refractory benign biliary anastomotic strictures, Cardiovasc. Intervent. Radiol. 43 (2020) 749–755, https://doi.org/10.1007/s00270-020-02442-4.

[6] S. Rejchrt, M. Kopacova, J. Brozik, J. Bures, Biodegradable stents for the treatment of benign stenoses of the small and large intestines, Endoscopy 43 (2011) 911–917, https://doi.org/10.1055/s-0030-1256405.

[7] L. Novotny, M. Crha, P. Rauser, A. Hep, J. Misik, A. Necas, D. Vondrys, Novel biodegradable polydioxanone stents in a rabbit airway model, J. Thorac. Cardiovasc. Surg. 143 (2012) 437–444, https://doi.org/10.1016/j.jtcvs.2011.08.002.

[8] L. Stehlik, V. Hytych, J. Letackova, P. Kubena, M. Vasakova, Biodegradable polydioxanone stents in the treatment of adult patients with tracheal narrowing, BMC Pulm. Med. 15 (2015) 164, https://doi.org/10.1186/s12890-015-0160-6.

[9] B.T. Griffiths, P. James, G. Morgan, A. Diamantopoulos, A. Durward, A. Nyman, Biodegradable stents for the relief of vascular bronchial compression in children with left atrial enlargement, Journal of bronchology & interventional pulmonology 27 (2020) 200–204, https://doi.org/10.1097/lbr.0000000000000654.

[10] M.M. Hirdes, P.D. Siersema, P.G. van Boeckel, F.P. Vleggaar, Single and sequential biodegradable stent placement for refractory benign esophageal strictures: a prospective follow-up study, Endoscopy 44 (2012) 649–654, https://doi.org/10.1055/s-0032-1309818.

[11] M.W. van den Berg, D. Walter, E.M. de Vries, F.P. Vleggaar, M.I. van Berge Henegouwen, R. van Hillegersberg, P.D. Siersema, P. Fockens, J.E. van Hooft, Biodegradable stent placement before neoadjuvant chemoradiotherapy as a bridge to surgery in patients with locally advanced esophageal cancer, Gastrointest. Endosc. 80 (2014) 908–913, https://doi.org/10.1016/j.gie.2014.06.004.

[12] Ó. Nogales, A. Clemente, A. Caballero-Marcos, J. García-Lledó, L. Pérez-Carazo, B. Merino, M. López-Ibáñez, M.D. Pérez Valderas, R. Bañares, C. González-Asanza, Endoscopically placed stents: a useful alternative for the management of refractory benign cervical esophageal stenosis, Rev. Esp. Enferm. Dig. : organo oficial de la Sociedad Espanola de Patologia Digestiva 109 (2017) 510–515, https://doi.org/10.17235/reed.2017.4795/2016.

[13] J.A. Martins, A.A. Lach, H.L. Morris, A.J. Carr, P.-A. Mouthuy, Polydioxanone implants: a systematic review on safety and performance in patients, J. Biomater. Appl. 34 (2020) 902–916, https://doi.org/10.1177/0885328219888841.

[14] E.D. Boland, B.D. Coleman, C.P. Barnes, D.G. Simpson, G.E. Wnek, G.L. Bowlin, Electrospinning polydioxanone for biomedical applications, Acta Biomater. 1 (2005) 115–123, https://doi.org/10.1016/j.actbio.2004.09.003.

[15] N. Goonoo, R. Jeetah, A. Bhaw-Luximon, D. Jhurry, Polydioxanone-based biomaterials for tissue engineering and drug/gene delivery applications, Eur. J. Pharm. Biopharm. 97 (2015) 371–391, https://doi.org/10.1016/j.ejpb.2015.05.024.

[16] K.-K. Yang, X.-L. Wang, Y.-Z. Wang, Poly (p-dioxanone) and its copolymers, J. Macromol. Sci. Polym. Rev. 42 (2002) 373–398, https://doi.org/10.1081/MC-120006453.

[17] H. Kricheldorf, D.O. Damrau, Polylactones, 42. Zn l-lactate-catalyzed polymerizations of 1, 4-dioxan-2-one, Macromol. Chem. Phys. 199 (1998) 1089–1097, https://doi.org/10.1002/(SICI)1521-3935(19980601)199:6<1089::AID-MACP1089>3.0.CO;2-S.

[18] S. Kumbar, C. Laurencin, M. Deng, Natural and Synthetic Biomedical Polymers, Newnes, 2014.

[19] S. Gestí, B. Lotz, M.T. Casas, C. Alemán, J. Puiggali, Morphology and structure of poly (p-dioxanone), Eur. Polym. J. 43 (2007) 4662–4674, https://doi.org/10.1016/j.eurpolymj.2007.08.007.

[20] J. Kurowiak, T. Klekiel, R. Będziński, Biodegradable polymers in biomedical applications: a review—developments, perspectives and future challenges, Int. J. Mol. Sci. 24 (2023) 16952.

[21] H.L. Lin, C. Chu, D. Grubb, Hydrolytic degradation and morphologic study of poly-p-dioxanone, J. Biomed. Mater. Res. 27 (1993) 153–166, https://doi.org/10.1002/jbm.820270204.

[22] J.C. Middleton, A.J. Tipton, Synthetic biodegradable polymers as orthopedic devices, Biomaterials 21 (2000) 2335–2346, https://doi.org/10.1016/s0142-9612(00)00101-0.

[23] M.A. Sabino, J.L. Feijoo, A.J. Müller, Crystallisation and morphology of poly(p-dioxanone), Macromol. Chem. Phys. 201 (2000) 2687–2698, https://doi.org/10.1002/1521-3935(20001201)201:18<2687::AID-MACP2687>3.0.CO;2-#.

[24] A. Bezrouk, T. Hosszu, L. Hromadko, Z. Olmrova Zmrhalova, M. Kopecek, M. Smutny, I. Selke Krulichova, J.M. Macak, J. Kremlacek, Mechanical properties of a biodegradable self-expandable polydioxanone monofilament stent: in vitro force relaxation and its clinical relevance, PLoS One 15 (2020) e0235842, https://doi.org/10.1371/journal.pone.0235842.

[25] C.-e. Wang, P.-h. Zhang, Design and characterization of PDO biodegradable intravascular stents, Textil. Res. J. 87 (2017) 1968–1976, https://doi.org/10.1177/0040517516660893.

[26] S. Rejchrt, M. Kopáčová, J. Bártová, Z. Vacek, J. Bureš, Intestinal biodegradable stents, Folia Gastroenterol Hepatol 7 (2009) 7–11.

[27] J. Loskot, D. Jezbera, A. Bezrouk, R. Doležal, R. Andrýs, V. Francová, D. Miškář, A. Myslivcová Fučíková, Raman spectroscopy as a novel method for the characterization of polydioxanone medical stents biodegradation, Materials 14 (2021), https://doi.org/10.3390/ma14185462.

[28] J. Loskot, D. Jezbera, Z.O. Zmrhalová, M. Nalezinková, D. Alferi, K. Lelkes, P. Voda, R. Andrýs, A.M. Fučíková, T. Hosszú, A complex in vitro degradation study on polydioxanone biliary stents during a clinically relevant period with the focus on Raman spectroscopy validation, Polymers 14 (2022) 938, https://doi.org/10.3390/polym14050938.

[29] P.J. Kahrilas, N.J. Shaheen, M.F. Vaezi, American Gastroenterological Association Institute technical review on the management of gastroesophageal reflux disease, Gastroenterology 135 (2008) 1392–1413, https://doi.org/10.1053/j.gastro.2008.08.044, 1413.e1391-1395.

[30] S. Fujimori, Gastric acid level of humans must decrease in the future, World J. Gastroenterol. 26 (2020) 6706–6709, https://doi.org/10.3748/wjg.v26.i43.6706.
[31] K. Tomihata, M. Suzuki, Y. Ikada, The pH dependence of monofilament sutures on hydrolytic degradation, J. Biomed. Mater. Res. 58 (2001) 511–518, https://doi.org/10.1002/jbm.1048.
[32] D. Greenwald, S. Shumway, P. Albear, L. Gottlieb, Mechanical comparison of 10 suture materials before and after in vivo incubation, J. Surg. Res. 56 (1994) 372–377, https://doi.org/10.1006/jsre.1994.1058.
[33] M. Kreszinger, O.C.f. Surgery, B. Toholj, A. B anski, S. Balpa, M. Cincovic, M. Pe in, M. Lipar, O. Smolec, Tensile strength retention of resorptive suture materials applied in the stomach wall - an in vitro study, Vet. Arh. 88 (2018) 235–243, https://doi.org/10.24099/vet.arhiv.170130.
[34] H.J. Kang, Y.S. Song, Effects of humidity and temperature on hydrolytic degradation of polydioxanone, Polym. Eng. Sci. 62 (2022) 2070–2078, https://doi.org/10.1002/pen.25989.
[35] D.V. Suárez-Vega, G.J. Velazco de Maldonado, R.L. Ortíz, V.J. García-Guevara, B. Miller-Kobisher, In vitro degradation of polydioxanone lifting threads in hyaluronic acid, J. Cutan. Aesthetic Surg. 12 (2019) 145–148, https://doi.org/10.4103/jcas.jcas_150_18.
[36] L.N. Woodard, M.A. Grunlan, Hydrolytic degradation and erosion of polyester biomaterials, ACS Macro Lett. 7 (2018) 976–982, https://doi.org/10.1021/acsmacrolett.8b00424.
[37] X. Liu, S. Feng, X. Wang, J. Qi, D. Lei, Y. Li, W. Bai, Tuning the mechanical properties and degradation properties of polydioxanone isothermal annealing, Turk. J. Chem. 44 (2020) 1430–1444, https://doi.org/10.3906/kim-2006-55.
[38] S.-W. Lee, S.-I. Kim, S.-J. Park, Solubility and density of p-dioxanone in organic solvent systems, Journal of Oil & Applied Science 25 (2008) 429–437, https://doi.org/10.12925/JKOCS.2008.25.4.3.
[39] H. Nishida, M. Yamashita, T. Endo, Y. Tokiwa, Equilibrium polymerization behavior of 1,4-Dioxan-2-one in bulk, Macromolecules 33 (2000) 6982–6986, https://doi.org/10.1021/ma000457t.
[40] R. Svoboda, J. Machotová, M. Krbal, D. Jezbera, M. Nalezinková, J. Loskot, A. Bezrouk, Complex thermokinetic characterization of polydioxanone for medical applications: conditions for material processing, Polymer 277 (2023) 125978, https://doi.org/10.1016/j.polymer.2023.125978.
[41] K. Ishikiriyama, M. Pyda, G. Zhang, T. Forschner, J. Grebowicz, B. Wunderlich, Heat capacity of poly-p-dioxanone, J. Macromol. Sci., Part B 37 (1998) 27–44, https://doi.org/10.1080/00222349808220453.
[42] M. Jaidann, J. Brisson, Conformation study of poly(p-dioxanone) fibers by polarized Raman spectroscopy, X-ray diffraction, and conformation analysis, J. Polym. Sci. B Polym. Phys. 46 (2008) 406–417, https://doi.org/10.1002/polb.21377.
[43] Y. Zheng, J. Zhou, F. Du, Y. Bao, G. Shan, L. Zhang, H. Dong, P. Pan, Formation of mesomorphic polymorph, thermal-induced phase transition, and crystalline structure-dependent degradable and mechanical properties of poly(p-dioxanone), Cryst. Growth Des. 19 (2019) 166–176, https://doi.org/10.1021/acs.cgd.8b01246.
[44] L. Ding, R.L. Davidchack, J. Pan, A molecular dynamics study of Young's modulus change of semi-crystalline polymers during degradation by chain scissions, J. Mech. Behav. Biomed. Mater. 5 (2012) 224–230, https://doi.org/10.1016/j.jmbbm.2011.09.002.